



OPEN

Ready-to-use nanopore platform for the detection of any DNA/RNA oligo at attomole range using an Osmium tagged complementary probe

Albert S. W. Kang¹, Janette G. Bernasconi¹, William Jack² & Anastassia Kanavarioti^{1✉}

Nanopores can serve as single molecule sensors. We exploited the MinION, a portable nanopore device from Oxford Nanopore Technologies, and repurposed it to detect any DNA/RNA oligo (target) in a complex mixture by conducting voltage-driven ion-channel measurements. The detection and quantitation of the target is enabled by the use of a unique complementary probe. Using a validated labeling technology, probes are tagged with a bulky Osmium tag (Osmium tetroxide 2,2'-bipyridine), in a way that preserves strong hybridization between probe and target. Intact oligos traverse the MinION's nanopore relatively quickly compared to the device's acquisition rate, and exhibit count of events comparable to the baseline. Counts are reported by a publicly available software, *OsBp_detect*. Due to the presence of the bulky Osmium tag, probes traverse more slowly, produce multiple counts over the baseline, and are even detected at single digit attomole (amole) range. In the presence of the target the probe is "silenced". Silencing is attributed to a 1:1 double stranded (ds) complex that does not fit and cannot traverse this nanopore. This ready-to-use platform can be tailored as a diagnostic test to meet the requirements for point-of-care cell-free tumor DNA (ctDNA) and microRNA (miRNA) detection and quantitation in body fluids.

Blood draw or other body fluid samples, known as liquid biopsies^{1–10}, contain pertinent information regarding the health status of an individual, the progress of a disease, whether or not an individual is disease-free after surgery, and even whether or not a certain therapy strategy seems promising². Liquid biopsies are far less invasive procedures than surgical/tumor biopsy. Body fluids contain cell-free DNA, a small fraction of which originates from the tumor. In 2016 the US Food and Drug Administration approved the first liquid biopsy test for EGFR-activating mutations in patients with non-small-cell lung cancer as a companion diagnostic test to enable therapy selection¹⁰. Cell-free DNA is believed to be fragmented and shorter in diseased individuals compared to healthy³. In addition to DNA, body fluids contain long non-coding RNAs¹¹, tRNA derived fragments¹², and other RNA oligos in the range of 20–300 nucleotides (nt). Among them is a group of single-stranded (ss) RNAs, 17–25 nt long, microRNAs or miRNAs^{13–15}. They were discovered 20 years ago and proven to be the tiny regulators that control the post-transcriptional expression of proteins^{16,17}; they are highly conserved and surprisingly stable in body fluids^{13,18}. Currently there are over 2300 human miRNAs known¹⁹, the subject of over 100,000 scientific publications. Up- or down-regulation of miRNAs is associated with various human diseases including cancer, heart disease, kidney disease, obesity, diabetes, etc.^{17,20}. miRNAs are proposed as biomarkers^{21,22} and as potential therapeutics²³ in personalized medicine. Body fluids contain trace amounts of ctDNA and miRNAs, that require simple, validated, and highly sensitive assays for testing^{8,9,24–27}. Current technologies for "small RNA" identification and quantitation, include microarray, NGS sequencing [Ion Torrent or Illumina (small RNA-seq)], and qRT-PCR-based methods that have been employed so far with great success^{24–27}. These technologies require substantial infrastructure and skilled personnel, are not well-suited for point-of-care testing and are out of the question for home testing. With our technology, this information could be easily accessible, even in the privacy of one's home.

The last 30 years have seen a surge in nanopore-based technologies using either solid-state or protein nanopores^{28–34}. In 2014 Oxford Nanopore Technologies (ONT) introduced and commercialized the first portable

¹Yenos Analytical LLC, 4659 Golden Foothill Pkwy, Suite 101, El Dorado Hills, CA 95672, USA. ²New England BioLabs, Inc., Ipswich, MA, USA. ✉email: tessi.kanavarioti@gmail.com

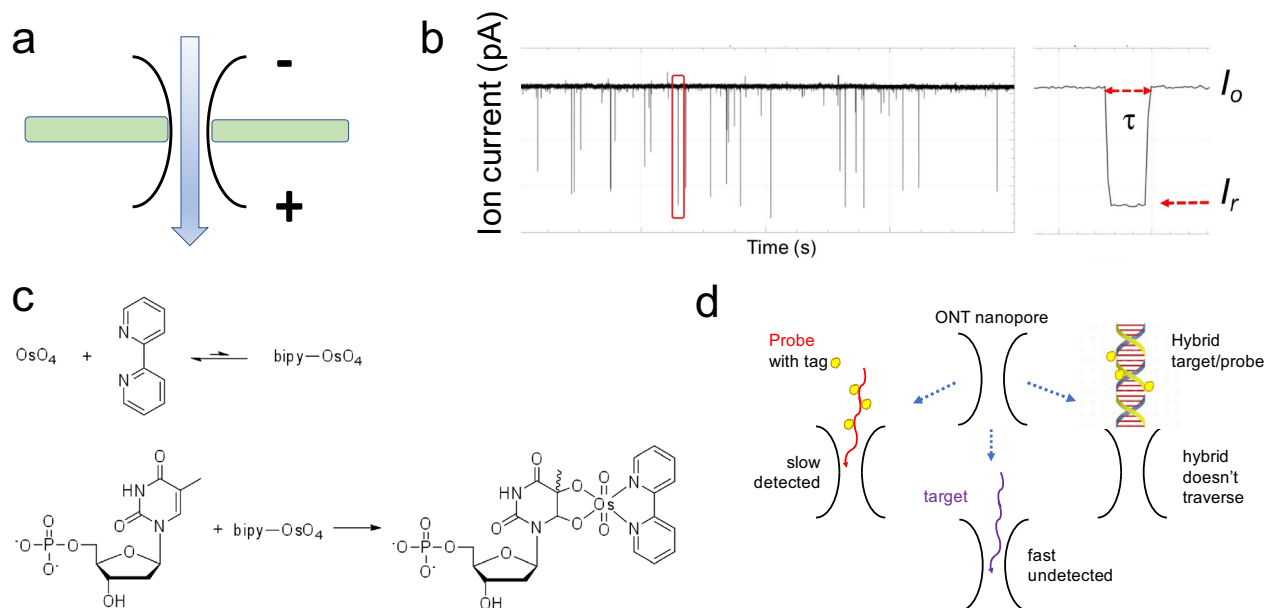


Figure 1. The critical parameters of the proposed diagnostic assay. **(a)** Schematic representation of a nanopore within a planar bilayer lipid membrane that separates two electrolyte filled compartments. Applying a constant voltage to the flow cell guides the passage of ions through the nanopore creating a measurable ionic current. **(b)** The $i-t$ trace obtained from a voltage-driven ion-channel experiment where the constant flow of electrolyte ions (I_o) via the pore is interrupted by the passage of molecules. These molecules appear as “events” with residual ion current I_r and residence time τ . **(c)** OsBp labeling reaction: OsO_4 and 2,2-bipyridine (bipy) have a low association constant, but their mixture adds to the C5-C6 double bond of pyrimidines and forms a stable conjugate, called here osmylated nucleic acid. The addition of OsBp creates a chromophore that absorbs in the range of 312 nm where native nucleic acids do not absorb (see “Experimental section”). **(d)** Cartoon illustrates the concept behind the proposed diagnostic test. ssDNA and ssRNA traverse the MinION’s CsGg nanopore and exhibit few counts because they traverse faster, compared to the device’s relatively slow acquisition rate; ds nucleic acids are too big and do not traverse this nanopore. Despite being bulkier than ss native nucleic acids, osmylated ss nucleic acids traverse the MinION/CsGg pore and produce numerous events. When an osmylated nucleic acid (probe) is added to a sample that contains its complementary (target), the probe and the target form a hybrid. When the target’s concentration is equal or higher than the probe’s concentration, the probe is hybridized. The probe is then prevented from traversing the pore, and few or no events are observed. The absence of target in the sample is evidenced by the numerous events produced by the probe while it freely traverses the pore.

nanopore device to sequence DNA and RNA practically anywhere, as long as a computer and internet are available³⁴. ONT technology is based on the CsGg protein nanopore³⁵, with sub 2 nm diameter, inserted in a planar lipid bilayer membrane that separates two electrolyte filled compartments (Fig. 1a). Applying a voltage across the two compartments leads to a constant flow of electrolyte ions (I_o) via the pore, recorded as a function of time ($i-t$). The passage of a single molecule through the pore reduces I_o to a lower level of residual ion current (I_r). This is recorded as an “event” with (I_r) and residence time (τ) (Fig. 1b). Currently the ONT platform is exclusively used for DNA/RNA sequencing³⁴, while comparable nanopore platforms are successfully employed for single molecule analyses^{36–51}. These and other studies, using experimental platforms, introduced nanopores to the arena of minimally invasive diagnostic assays.

The appeal of using nanopores as single molecule sensors resides in their ability to detect and count every molecule that traverses the pore. To appreciate this advantage, let us consider a 10 μL sample that contains miRNA21 at 10×10^{-15} M (10 femtoM or 10 fM) concentration. To the best of our knowledge, there is no method to analyze such diluted sample without amplification. This sample contains 1×10^{-19} mol, i.e. 0.1 attomole (amole), or approximately 60,000 molecules of miRNA21. A size-suitable nanopore may detect some, if not all, as long as there is an electrical field to guide them towards the pore and thread them through it. Compared to other analytical tools, nanopores appear highly fitting for trace analysis such as the DNA/RNA oligos in body fluids. The argument becomes even more compelling when there is a ready-to-use microfluidic device with an array of about 500 actively reporting nanopores which is the MinION configuration from ONT³⁴.

ONT commercialized portable nanopore devices that carry two types of flow cells; the MinION with 512 channels and the Flongle with 126 channels, all monitored simultaneously³⁴. ONT promotes these devices for direct sequencing of DNA and RNA with a minimum length of 200 nucleotides (nt)³⁴. In a recent study, attempts to sequence RNAs shorter than 200 nt following ONT protocol were unsuccessful⁵². In another study 100 nt

deoxyoligos were successfully sequenced by the MinION, albeit only after circularization and rolling circle amplification to produce long DNA with 100 nt repeats⁵³. Most of the DNA/RNA available in biological fluids is fragmented with lengths estimated in the range of 200 bp³ and miRNAs are very short¹⁶, and not amenable to direct ONT sequencing protocols. Still ONT devices/flow cells can be used for single molecule ion-channel measurements, just like any other nanopore. While several experimental nanopore platforms were successfully used for miRNA profiling (see later), we believe to be the first to show feasibility using a commercial device⁴⁹. The advantage compared to other platforms is that the ONT technology is accessible, ready-to-use, relatively inexpensive, and does not require any special skills or infrastructure.

We have exploited selective labeling of nucleic acids in an effort to enhance base-to-base discrimination^{41,44,49,54}, and used Osmium tetroxide 2,2'-bipyridine (OsBp) as the label/tag. OsBp is not reactive towards the purines and does not cleave the phosphodiester bond in DNA or RNA. OsBp adds to the C5–C6 double bond of the pyrimidines and forms two strong C–O bonds without cleaving the pyrimidine ring (Fig. 1c)^{55–60}. The products are named here “osmylated” nucleic acids. Reactivity of OsBp towards thymidine (T) is 28- and 7.5-times higher compared to the reactivity towards deoxycytidine (C) and deoxyuridine (U), respectively⁴⁴. We demonstrated control over the labeling conditions, and developed a protocol to selectively label T in the presence of the other pyrimidines⁵⁸. We developed capillary electrophoresis (CE) and High-performance Liquid chromatography (HPLC) methods to measure the extent of labeling in short and long DNA and RNA^{58,59} (“Experimental section”). We also conducted voltage-driven ion-channel measurements using SiN solid-state nanopores⁴¹, the α -Hemolysin nanopore⁴⁴, as well as the CsGg proprietary nanopore in the MinION⁴⁹, and demonstrated that all three platforms allow the translocation of osmylated nucleic acids, and clearly discriminate them from native nucleic acids. The discrimination is manifested as an event with markedly lower I_r and longer τ with increasing number of OsBp moieties (Fig. 1b). Here we exploit these features in order to single-out, detect, and count OsBp-tagged oligos in a complex mixture of native DNA and RNA.

Figure 1d illustrates the concept behind nanopore-based identification and quantification of a target oligo in a complex mixture; it is enabled by a custom-designed OsBp-tagged deoxyoligo (probe), that is complementary to the target. The use of a complementary oligo as a probe has been validated in several experimental nanopore platforms^{38,42,43,45,51}. These platforms however are made complicated by the fact that the probe is conjugated to a protein³⁸, a nanoparticle⁵¹, a homopolymer⁴², or a polypeptide⁴⁵. The detection in these platforms relies on counting the long blockades produced by the hybrid bumping at the nanopore entry and practically “getting stuck”. None of these methods reached commercial availability which hinders their broader use. In contrast to earlier approaches based on detection of the hybrid^{38,42,43,45,51}, our technology detects the translocation of the bulky osmylated probe facilitated by the relatively slow acquisition rate of the MinION (3.012 kHz sampling rate, equivalent to reporting 3 data points per 1 ms)³⁴. While the slow sampling rate misses most translocation events of native DNA/RNA oligos, the events corresponding to the translocation of our tagged probes are detected. In the absence of the target, the probe traverses the nanopore and produces a detectable event. In the presence of the target, the probe forms a 1:1 ds complex (hybrid) with the target. The hybrid does not fit and cannot traverse the proprietary CsGg nanopore of the ONT devices³⁴ (Fig. 1d). Hence the probe is “silenced”. The hybrid does not prevent ss nucleic acids going through the pore, as ONT technology incorporates automatic reversal of voltage to free the nanopores from such unproductive occurrences. Therefore, to test the presence/absence of a target oligo in a sample, a probe is simply added to the sample and the mixture is tested in an ONT device by conducting voltage-driven single molecule experiments. Absence of the target oligo in a sample is conjectured from the observation of numerous events due to the probe’s translocation via the pore. The presence of the target oligo in a sample is concluded from the absence of events, due to hybrid formation between the probe and the target. Quantification of the target is based on the known concentration of the probe and the 1:1 hybrid formation. The concept is neither unique to the Osmium tag nor to the ONT nanopore array. Any bulky tag with selectivity for one of the bases should yield comparable behavior to what is observed with OsBp. In addition, most nanopore platforms with dimensions that allow the translocation of ss nucleic acids and prevent the translocation of ds nucleic acids will conform to the concept described in Fig. 1d, under suitable conditions of applied voltage and data acquisition speed.

Results and discussion

The materials used in this study are all synthetic oligos of the highest purity and are listed in Table 1. Osmylation protocols were developed by us. Intact and osmylated nucleic acids were further characterized in-house by validated HPLC methods^{59,61} (see “Experimental section”). Nanopore experiments were conducted using the ONT devices and the ONT supplied Flush buffer (ONT buffer or buffer), in addition to company’s instructions of how to prime the flow cell, add the sample, select voltage, and acquire the raw $i-t$ traces. No sample library was prepared and no enzyme-assistance was exploited. Samples were prepared in 90–95% ONT buffer, unless otherwise noted. The nanopore experiments reported here were conducted at the factory-preset, flow cell temperature in the range of 34–35 °C. The raw $i-t$ traces of all channels (a *fast5* file) were captured and analyzed using *OsBp_detect* software⁶² (see “Experimental section”). The output, a *tsv* file, is read using Microsoft Excel. It lists I_o value for each channel, as well as the selected events and their I_r value from which I_r/I_o is calculated. It also lists the times, in data time points, of the beginning and of the end of each event (see Fig. S1, Supplementary Information). *OsBp_detect* permits manual setting of parameters, in order to select events of interest⁶². Here we selected events with residence time $4 \leq \tau \leq 300$ data time points or the equivalent $1.3 \leq \tau \leq 100$ ms, and fractional residual ion current $I_r/I_o \leq 0.55$ (Fig. 1b). Figures 2, 4, 5, 6 and 7 present histograms of count of events (abbreviated as counts or events) as a function of I_r/I_o using a 0.05 bin.

Nanopore experiments using the Flongle flow cell. Figure 2 illustrates results exploiting the Flongle flow cell. Figure 2a was a first attempt to observe a hybrid. It was known from earlier work with the MinION flow cell that T8, a 32 nt RNA with 9 pyrimidines and a total of 8 OsBp tags (see sequence in Table 1), requires high voltage to traverse, exhibits multiple translocation events, and severely obstructs the ionic current exhibiting a maximum of counts at $(I_r/I_o)_{\max} \approx 0.1$. Repeating the experiment practically duplicated the earlier work on the MinION⁴⁹. Even though not a perfect complement, we used $d(\text{TC})_{10}$ to form the ds complex, as $d(\text{CT})_{10}$ can base-pair 16 out of 20 nt, including 8 GC pairs, with T8. While the experiment with probe T8 exhibited, on average, 400 events per channel, the experiment using a 1:1 mixture of probe T8 and $d(\text{CT})_{10}$, yielded less than 50 events per channel for some channels and zero events reported for the rest of the channels (see Figs. S1, S2 in Supplementary Information). Figure 2b illustrates a test for identification of miRNA122⁶³. The probe used here is dmiR122, the exact deoxy complement of miRNA122, and carries 4T(OsBp) (see Table 1). The sample with probe dmiR122 alone exhibited numerous counts, while the sample with an approximate equimolar mixture of this probe and miRNA122 exhibited markedly fewer counts. A third sample with a 4-times higher miRNA load, composed of miRNA21^{64–68} and miRNA140⁶³ also exhibited fewer counts compared to the probe sample. The latter suggests that identification of a target in a complex mixture of miRNAs with excess non-target components is plausible. These as well as other experiments (see later) demonstrate the feasibility of the concept presented in Fig. 1d. They also reveal that both the target and the probe can be either RNA or DNA, the difference being that probes are osmylated oligos, while targets are not. Here we focused on probes that are DNA oligos, because of the lower cost and the higher synthetic product quality compared to RNA oligos.

Alternative methods to test hybridization between a target and its probe. We sought independent means to test hybridization between osmylated nucleic acids and their DNA or RNA targets. Enzymatic DNA polymerase elongation of an unmodified primer using partially osmylated template ssM13mp18 was our first attempt to obtain support for hybridization, but elongation of primers was not detectable. None of the osmylated templates exceeded 2% of the incorporation seen with unmodified M13mp18 (Table S1 in the Supplementary Information). We then tested unmodified ssM13mp18, as the template, and used 30 nt long, osmylated at the thymidine [T(OsBp)] primers, BJ1, BJ2, BJ3, and BJ4 (see Table 1). BJ1 carries the identical sequence of primerM13for(–20) at the 3′ end, and is extended by 13 nt at the 5′ end. BJ2 carries the identical sequence of primerM13for(–41) at the 3′ end, and is extended by 6 nt at the 5′ end. BJ3 and BJ4 have the identical sequence to BJ2 with the exception of one mismatch in the middle of the sequence. Even though BJ2, BJ3, and BJ4 carried 6, 5, and 7T(OsBp) bases, respectively (table, 3rd column), they were all successfully elongated (Fig. 3a), suggesting that T(OsBp) did not prohibit 1:1 hybridization between intact ssM13mp18 and the probes. In contrast, BJ1, with 6 T(OsBp) did not elongate, presumably due to the presence of a T(OsBp) base at the 3′ end and the inability of the enzyme to add a nucleotide to it (Fig. 3a). Control experiment mixing BJ1 with M13(fwd6097) 1:1 displayed full incorporation, discounting soluble inhibitors as the cause of low incorporation with BJ1 (Fig. 3a). Still absence of elongation with BJ1 does not necessarily imply absence of hybridization.

These elongation experiments were done at salt concentration presumed to be much lower than the one used for the nanopore experiments, they were limited to ssM13mp18 and to the use of probes with sequences identical to known primers. To extend hybridization tests to miRNAs and any DNA/RNA oligo we developed an HPLC method (see “Experimental section”). This HPLC method is based on the HPLC method we use to test for oligo purity with the following modifications: it uses (1) ONT buffer as the sample solvent and (2) HPLC column temperature at 35 °C to mimic the ONT working flow cell temperature. It should be noted that the HPLC column packing may interfere with hybridization, and therefore all the HPLC-based results are purely suggestive. Having said that, there was no instance in our work where the HPLC results and the nanopore experiment contradicted each other. To confirm hybridization HPLC analyses of three separate samples are required. These three samples contain (1) the probe, (2) the target, and (3) the sample with the 1:1 mixture of the two components that contains the presumed hybrid (see Figs. 3b–d). Absence of hybridization is consistent with an HPLC profile of the mixture sample that closely overlaps with the “sum” of the HPLC profiles of the two components (Fig. 3c). Evidence for hybridization is consistent with a hybrid peak that elutes well resolved from the peaks of the target and of the probe and typically 1–1.5 min later than either probe or target. In addition, the probe and hybrid peaks exhibit absorbance at 312 nm, due to the presence of the OsBp tag, but the target peak does not (see “Experimental section”). We intentionally prepared 1:1 mixture samples with a small excess of the target to prevent the probe from being in excess. This is why in many of the HPLC chromatograms the analysis of the hybrid sample includes a smaller peak attributed to the target, in addition to the large peak attributed to the hybrid.

Figure 3b shows the HPLC chromatograms of samples where both oligos are unmodified nucleic acids. Here the HPLC profile of the sample with the 1:1 mixture is consistent with strong hybridization, based on the features discussed above. Figure 3d is a repeat of the HPLC analyses in Fig. 3b, only that BJ2 is now osmylated; it is a probe. The corresponding HPLC profile of the 1:1 mixture in Fig. 3d is also consistent with strong hybridization. The same HPLC method indicated that miRNA21 and probe 21EXT (see Table 1) do not hybridize (Fig. 3c). The absence of hybridization in Fig. 3c is attributed to the many OsBp moieties on probe 21EXT, a total of 8 T(OsBp) with 6 T(OsBp) found within the 22 nt sequence of the probe which is complementary to the target. Additional hybridization tests confirmed the hypothesis that ds complex formation is prohibited or disfavored in the presence of a large number of OsBp moieties on the probe (see Fig. S3 in the Supplementary Information). Besides the number of OsBp moieties in a molecule, the actual location matters as well. As seen with the BJ1–4 probes, hybridization remains strong, despite a relatively large number of T(OsBp). This is most likely because these tags occupy a small area of the sequence, leaving two rather long subsequences available for duplex formation with the target.

ID, DNA unless identified as RNA	Sequence; sequences are all deoxyribose, unless identified as RNA in the 1 st column; (mU is 2'-OMeU)	T/total nt	Theoretical R(312/272) ¹ T(OsBp) only	Observed R(312/272) ²	Py/total nt	No of OsBp ³ on average	Figure
PrimerM13for(-20)	GTA AAA CGA CGG CCA GT	2/17	0.235	0.230°	6/17	1.955°	S8
PrimerM13for(-41)	CGC CAG GGT TTT CCC AGT CAC GAC	5/24	0.417	0.416°	14/24	4.992°	S8
PrimerM13rev(-27)	CAG GAA ACA GCT ATG AC	2/17	0.235	0.236°	6/17	2.006°	S8
PrimerM13rev(-48)	AGC GGA TAA CAA TTT CAC ACA GG	4/23	0.348	0.326°	9/23	3.749°	S8
Complement primer-M13for(-20)	TTG GCA CTG GCC GTC GTT TTA CAA CGT CGT GAC TG	11/35	0.629	0.578°	20/35	10.115°	S10
BJ1	CAG TCA CGA CGT TGT AAA ACG ACG GCC AGT	5/30	0.333	0.295° 0.327 ^b	13/30	4.425° 4.905 ^b	S9
BJ1EXT(mU)	TTT GmUA AAA CGA CGG CCA GmUA AA	3/23	0.261	0.273 ^b	9/30	3.140 ^b	S9
Complement primer-M13for(-41)	ACA ACG TCG TGA CTG GGA AAA CCC TGG CGT TAC CC	6/35	0.333	0.344°	17/35	6.020°	S10
BJ2	GGG TAA CGC CAG GGT TTT CCC AGT CAC GAC	6/30	0.400	0.401° 0.401 ^b	15/30	6.015° 6.015 ^b	S9
BJ3	GGG TAA CGC CAG GGT TTC CCC AGT CAC GAC	5/30	0.333	0.347° 0.353 ^b	15/30	5.205° 5.295 ^b	S9
BJ4	GGG TAA CGC CAG GGT TTT TCC AGT CAC GAC	7/30	0.467	0.452° 0.445 ^b	15/30	6.780° 6.675 ^b	S9
BJ2 TA(OMe)	TTT CGC CAG GGU UUU CCC AGU CAC GAC AAA (all 2'-OMe with the exception of Ts)	3/30	0.200	0.324 ^a	17/30	4.860 ^a	S11
BJ2 AT(OMe)	AAA CGC CAG GGU UUU CCC AGU CAC GAC TTT (all 2'-OMe with the exception of Ts)	3/30	0.200	0.311 ^a	17/30	4.665 ^a	S11
BJ2EXT(mU)	TTT CGC CAG GmU mUmUmU CCC AGmU CAC GAC AAA	3/30	0.200	0.278 ^b	17/30	4.170 ^b	S11
miRNA21, RNA	UAG CUU AUC AGA CUG AUG UUG A	0/22	–	0.268 ^c	11/22	2.950 ^c	S12
miRNA21-A ₁₅ , RNA	UAG CUU AUC AGA CUG AUG UUG A ₁₆	0/37	–	0.099°	11/37	1.832°	S12
Complement miRNA-21, RNA	UCA ACA UCA GUC UGA UAA GCU A	0/22	–	0.183 ^c	11/22	2.013 ^c	S18
dmiR21	TCA ACA TCA GTC TGA TAA GCT A	6/22	0.545	0.485°	11/22	5.339°	S13
21EXT	TTT CAA CAT CAG TCT GAT AAG CTA	8/24	0.667	0.665°	13/24	8.000°	S13
dmiR21(OMe)	UCA ACA UCA GUC UGA UAA GCU A (all 2'-OMe)	0/22	–	0.082 ^b 0.124 ^c 0.26 ^d	11/22	0.902 ^b 1.365 ^c 2.85 ^d	S14
21EXT(mU)	TTT CAA CAmU CAG mUCmU GAmU AAG CmU AAA	3/27	0.231	0.433 ^a 0.344 ^b	13/27	5.846 ^a 4.644 ^b	S14
miRNA122, RNA	UGG AGU GUG ACA AUG GUG UUU G	0/22	–	0.277 ^c	9/22	3.04 ^c	S12
Complement miRNA122, RNA	CAA ACA CCA UUG UCA CAC UCC A	0/22	–	0.143 ^c	13/22	1.573 ^c	S18
dmiR122	CAA ACA CCA TTG TCA CAC TCC A	4/22	0.364	0.404°	13/22	4.444°	S15
2XdmiR122	(CAA ACA CCA TTG TCA CAC TCC A) ₂	8/44	0.364	0.380°	26/44	8.36°	S15
122EXT	TTT CAA ACA CCA TTG TCA CAC TCC A	7/25	0.560	0.602°	16/25	7.525°	S15
dmiR122(OMe)	C AAA CAC CAU UGU CAC ACU CCA (all 2'-OMe)	0/22	–	0.088 ^b 0.150 ^c	13/22	0.965 ^b 1.654 ^c	S15
miRNA140, RNA	CAG UGG UUU UAC CCU AUG GUA G	0/22	–	0.233 ^c	12/22	2.563 ^c	S12

Continued

ID, DNA unless identified as RNA	Sequence; sequences are all deoxyribose, unless identified as RNA in the 1 st column; (mU is 2'-OMeU)	T/total nt	Theoretical R(312/272) ¹ T(OsBp) only	Observed R(312/272) ²	Py/total nt	No of OsBp ³ on average	Figure
dmiR140	CTA CCA TAG GGT AAA ACC ACT G	4/22	0.364	0.357 ^o	10/22	3.926 ^o	S16
2XdmiR140	(CTA CCA TAG GGT AAA ACC ACT G) ₂	8/44	0.364	0.321 ^o	20/44	7.055 ^o	S16
140EXT(mU)	TTT CmUA CCA mUAG GGmU AAA ACC ACmU GAA	3/27	0.222	0.374 ^a	13/27	5.049 ^a	S16
				0.314 ^b		4.239 ^b	
d(CT) ₁₀	CTCTCTCTCTCTCTC TCTCT	10/20	1.00	1.044 ^b	20/20	10.44 ^b	S17
T8, RNA	(AG) ₄ C ₂ (AG) ₄ C ₂ (AG) ₃ CCU UCA, note 4	0/32	–	0.50	9/32	8.0	–
100 nt RNA	Note 5	0/100	–	0.239 ^c		11.96 ^c	S17
100 nt RNA(OMe)	Note 6; identical sequence to 100 nt RNA, but some 2'-OMe	0/100	–	0.224 ^c		11.19 ^c	S17

Table 1. List of tested DNA or RNA oligos. The 3 miRNAs tested here have the sequence of the corresponding miRNA-5p. Oligo ID, sequence, number of thymidines over total nucleotides (T/total nt), number of pyrimidines over total nucleotides (Py/nt), theoretical R(312/272) for T(OsBp) (see footnote and “Experimental section”), Observed R(312/272) is the ratio of the observed areas under the HPLC peak at 312 nm over the area at 272 nm; HPLC analytical profiles for each oligo and its osmylated conjugate (Fig. S#) are included in the Supplementary Information. The number of Py(OsBp) or OsBp moieties, on average, depends on the protocol used for osmylation and is calculated as described in footnote 3. Underlined partial sequences correspond to M13primers with or without a mismatch. ¹Theoretical R(312/272) for T only equals $2 \times (\text{No of T})/(\text{total nt})$ (see “Experimental section”). ²Observed R(312/272) is the observed Absorbance at 312 nm divided by the observed absorbance at 272 nm from HPLC. Observed R(312/272) = $2 \times (\text{No of Py(OsBp)})/(\text{total nt})$ (see “Experimental section”). ³No of OsBp, on average, is determined from the equation above, and it is equal to observed R(312/272)x(total nt)/2. ^{o,a,b,c,d} are different protocols for preparing osmylated oligos: ^o batch of OsBp stock solution prepared without dissolving bipy ahead of OsO₄ addition, 40 min with 2.6 mM OsBp. ^{a,b,c} batch of OsBp stock solution prepared by dissolving bipy before adding OsO₄; ^a45 min with 2.6 mM OsBp; ^b30 min with 2.6 mM OsBp; ^c30 min with 3.9 mM OsBp. ^dSpecial protocol (30 min with 5.25 mM OsBp) to add about 3 OsBp per 22 nt oligo in the absence of Ts. Note 4: Practically 100% osmylated at all pyrimidines, from reference 49. Note 5: 100 nt RNA sequence: 5'-UUA CAG CCA CGU CUA CAG CAG UUU UAG AGC UAG AAA UAG CAA GUU AAA AUA AGG CUA GUC CGU UAU CAA CUU GAA AAA GUG GCA CCG AGU CGG UGC UUU U-3'. Note 6: 100 nt RNA(OMe) sequence: 5'-mUmUmA CAG CCA CGU CUA CAG CAG UUU UAG AmGmC mUmAmG mAmAmA mUmAmG mCAA GUU AAA AUA AGG CUA GUC CGU UAU CAmA mCmUmU mGmAmA mAmAmA mGmUmG mGmCmA mCmCmG mAmGmU mCmGmG mUmGmC mUmUmU mU-3'; m stands for 2'-OMe.

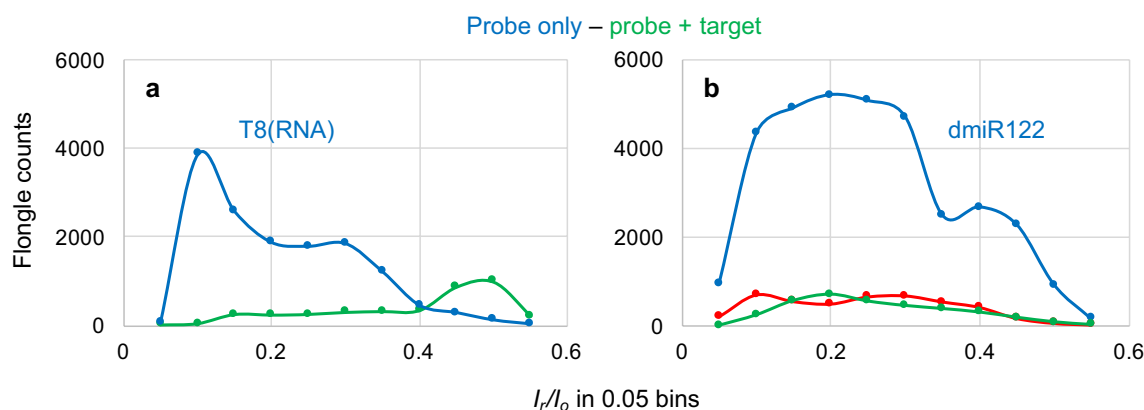


Figure 2. Voltage-driven ion-channel (nanopore) experiments conducted with the Flongle ONT device; samples in >90% ONT buffer. (a) 1 h at -200 mV using the same Flongle flow cell: (1) $5 \mu\text{M}$ probe T8(RNA) (blue trace) and (2) $5 \mu\text{M}$ each a mixture of T8(RNA) and d(CT)₁₀ (green trace). It is noticeable that these two molecules are only partially complementary to each other. Count of events (counts) were obtained using the *OsBp_detect* software to analyze and report the raw *fast-5* file data acquired with MINKNOW (see “Experimental section”). Counts are plotted as a function of I_p/I_o with a bin size of 0.05. (b) 2 h at -190 mV using the same Flongle flow cell: (1) $5 \mu\text{M}$ probe dmiR122 (blue trace), (2) $5 \mu\text{M}$ each a mixture of dmiR122 and miRNA122 (green trace), and (3) 1 h at -180 mV a mixture $10 \mu\text{M}$ each of miRNA122 and miRNA140 (red trace) using a different Flongle flow cell. It is noticeable that dmiR122 carries 4 OsBp moieties and its sequence is perfectly complementary to miRNA122. Data acquisition and analysis as described under (a).

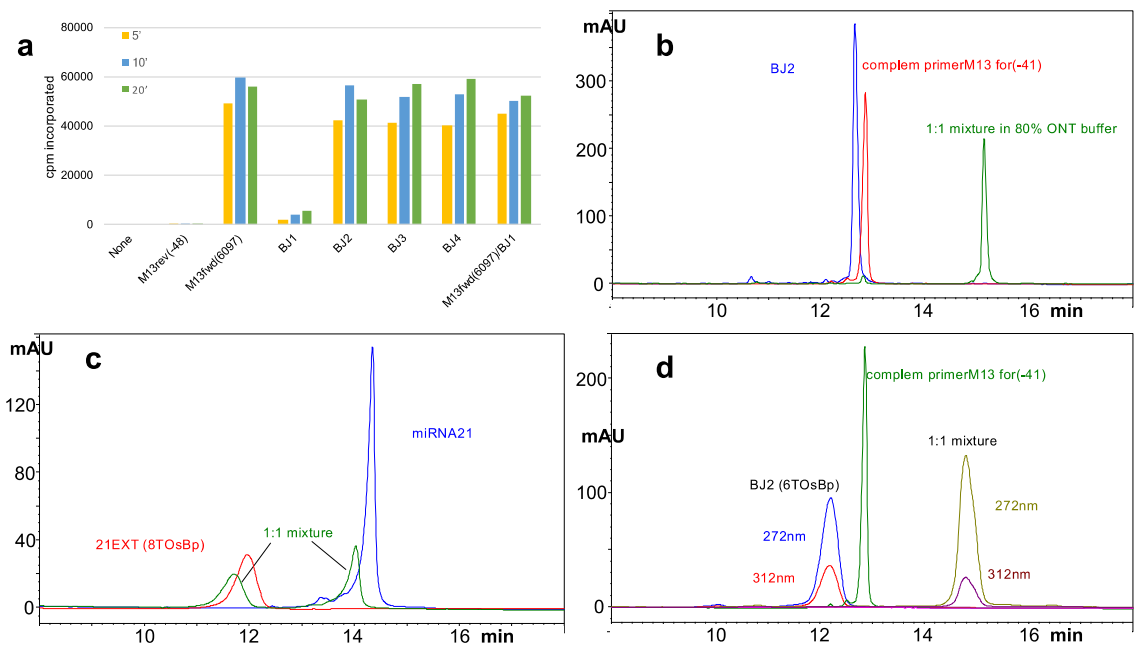


Figure 3. Alternative approaches to testing hybridization between osmylated probes and targets. **(a)** Enzymatic elongation of osmylated primers using ssM13mp18 DNA as the template and DNA polymerase; time points obtained at 5, 10 and 20 min. No primer and M13rev(-48) used as negative controls. With the exception of BJ1, all the other osmylated primers exhibit enzymatic elongation comparable to the positive control M13fwd(6097). Absence of elongation with BJ1 is attributed to the presence of a T(OsBp) at the 3' end. Experiment shown at the far right of the graph, done with a 1:1 mixture of BJ1 and the positive control indicates that any components/ traces present in the BJ1 preparation after osmylation were NOT responsible for inhibiting the elongation of BJ1. **(b–d)** Overlapping HPLC profiles from the analyses of different samples, with samples at about 5 μ M in about 90% ONT buffer. The same HPLC method B was used for all the samples (see “Experimental section”). Intact ss oligos and ds oligos appear as sharp peaks, whereas osmylated oligos and hybrids with one osmylated strand appear as broad peaks; hybrids elute later compared to ss nucleic acids. **(b)** Sample composition: intact BJ2 (blue trace), intact complement of primerM13for(-41) (red trace). The HPLC profile of their equimolar mixture is consistent with hybridization (green trace). **(c)** Sample composition: miRNA21 (blue trace), probe 21EXT carrying 8 dT(OsBp) moieties (red trace), and equimolar mixture of the two (green trace). HPLC profile of the mixture consistent with NO hybridization, attributed to the high number of single OsBp tags, 6 within a sequence of 22 nt, likely to distort the helical structure of the probe, and prevent ds formation. **(d)** Sample composition practically the same as under **(b)**, with the exception that in these samples BJ2 carries 6 dT(OsBp) moieties (first peak with broad shape and absorbance at 312 nm). HPLC profile of the mixture is consistent with hybridization, attributed to the fact that most of the OsBp moieties are adjacent, so that the rest of the sequence can still hybridize with the target.

Hybridization silences the probe in the presence of the DNA oligo target. Experiments in Fig. 2 were conducted using probe, target, and hybrid concentration in the 5 μ M range. Since sample size of a MinION and that of a Flongle flow cell is 75 μ L vs. 30 μ L, the 5 μ M concentration corresponds to a 0.38 vs. a 0.15 nmole sample load, respectively. It is worth mentioning that sample load for a nanopore experiment is not the same as sample load for an HPLC analysis, as the HPLC injection volume is typically not the same as the flow cell sample size. Figure 4a illustrates the HPLC hybridization test, described above, using probe BJ1 with 5 T(OsBp) and its target, complementary primer M13for(-20). The samples of probe and hybrid were used, as is, for the nanopore experiments, shown in Fig. 4b. We note that probe BJ1 was not enzymatically elongated using ssM13mp18, as the template, which we attributed to the presence of a T(OsBp) base at the 3' end. In Fig. 4 hybridization is documented both by HPLC analysis and by nanopore experiments, as shown by the huge drop in the number of counts reported for the hybrid sample (green trace) compared to the counts reported with the probe sample (solid blue trace). The effect is dramatic for the $(I_r/I_o)_{\max}$ and clearly detectable for the rest of the I_r/I_o range.

Applied voltage is a critical parameter. Figure 4b illustrates that testing probe BJ1 with applied voltage at -180 mV exhibits very low counts suggesting that probe translocation is inefficient at -180 mV (dashed blue trace). Without addition of a new sample, raising the voltage to -210 mV (solid blue trace) yielded dramatically more counts compared to the counts obtained at -180 mV. Figure S4 (left figure, Supplementary Information) illustrates that probes BJ2 and BJ4 follow the same pattern as BJ1. We attribute this observation to the presence of adjacent dT(OsBp) in these probes, and the notion that dT(OsBp) exhibits the lowest observed $(I_r/I_o)_{\max}$ among all tested pyrimidines, a strong indication of heavy crowding. Heavy crowding in adjacent OsBp moieties was concluded from earlier studies using RNAs and the MinION/CsGg⁴⁹, as well as DNAs and the α -Hemolysin

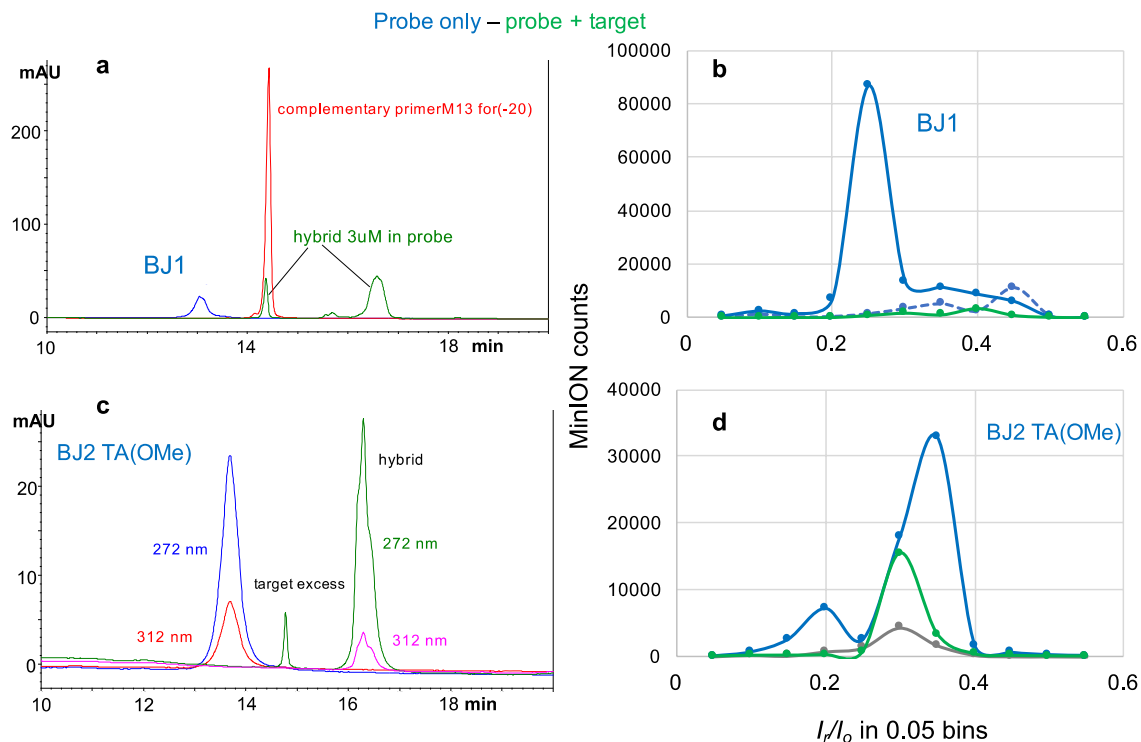


Figure 4. Same samples tested by HPLC and by nanopore; samples in >90% ONT buffer. **(a)** Overlapping HPLC profiles of samples, at about 0.2 nmoles, in ONT buffer (1) probe BJ1 (blue trace), (2) target (red trace) shown here at a much higher load, and (3) mixture of probe at about 0.2 nmoles and target with about 30% excess over the probe (hybrid, green trace). The HPLC profile of the mixture is consistent with hybridization. **(c)** Overlapping HPLC profiles (1) of the probe BJ2 TA(OMe) at about 0.2 nmole load and (2) its approximately equimolar mixture with the complementary target, complementary primerM13for(-41). Target identified as a small peak, at 5% excess over the probe. The HPLC profile of the mixture (hybrid, green trace) is consistent with ds formation (see text). HPLC profiles for these two samples are shown at both the 272 and 312 nm (see text and “Experimental section”). **(b,d)** One hour long nanopore experiments conducted with a MinION flow cell using the same samples as in **(a,c)**, respectively; samples in **(b)** were used as is, while samples in **(d)** were used after a 1000-fold or a 100-fold dilution in ONT buffer. **(b)** Probe BJ1 was tested at -180 mV (dashed blue trace) and showed few counts. No sample was added, the voltage was raised to -220 mV and an additional nanopore experiment was conducted at -220 mV (solid blue trace) with counts exceeding 100,000. In contrast to the counts obtained with BJ1, the hybrid sample exhibited very few counts (tested 1 h at -190 mV, green trace). **(d)** Nanopore experiments using the same flow cell: (1) control/buffer test (0.75 h tested at -180 mV, grey trace), (2) probe BJ2 TA(OMe) at 0.38 pmole load (2 h tested at -210 mV, blue trace), (3) equimolar mixture of probe and target at 3.8 pmole load each (1 h tested at -210 mV, green trace). The observation of lower counts with the hybrid sample compared to the probe sample suggest target identification for either **(b,d)**, in agreement with the HPLC results. The nanopore experiment with BJ2 TA(OMe) probe at the 0.38 pmole load suggests probe detectability at the sub-pmole level. The experiment with the hybrid sample in **(d)** indicates that the hybrid endures under the experimental conditions of duration and applied voltage (see text). Data acquisition and analysis as described under Fig. 2a.

nanopores⁴⁴. Since our probes are deoxyoligos and include several T bases in the sequence, the steric hindrance is compounded. Labeled nucleic acids may approach the CsGg pore guided by the applied voltage drop, but to traverse the pore a certain minimum voltage is required. Multiple experiments suggested that the applied voltage for efficient translocation of most of our probes via the proprietary CsGg nanopore is in the range of -210 ± 10 mV. In contrast to the observations with the probes, intact DNA oligos exhibit insignificant counts^{44,49}, as shown also here in Fig. S4 (right figure, Supplementary Information). Target/unmodified miRNAs exhibit measurable counts with a slight decreasing trend as a function of increasing voltage (Fig. S5 in the Supplemental Information). This is consistent with the expectation that increased voltage results in faster translocation and faster translocation, in turn, results in missed events, as the acquisition rate of the device remains constant at 3 data points per ms. In order to make the counts with native RNAs detectable the total load was 4-times higher than the highest probe load. Experiments with voltage higher than -220 mV were not conducted, in order to protect the protein pores that, in our experience, did not last as long at -220 mV compared to -180 mV. The observation that our probes practically do not traverse the CsGg pore at -180 mV is an advantage for a diagnostic test. It provides the opportunity to deplete the sample from excess non-target nucleic acids at -180 mV, and then, without adding a new sample, raise the voltage at -220 mV in order to detect, or not, the presence of the uncomplexed probe.

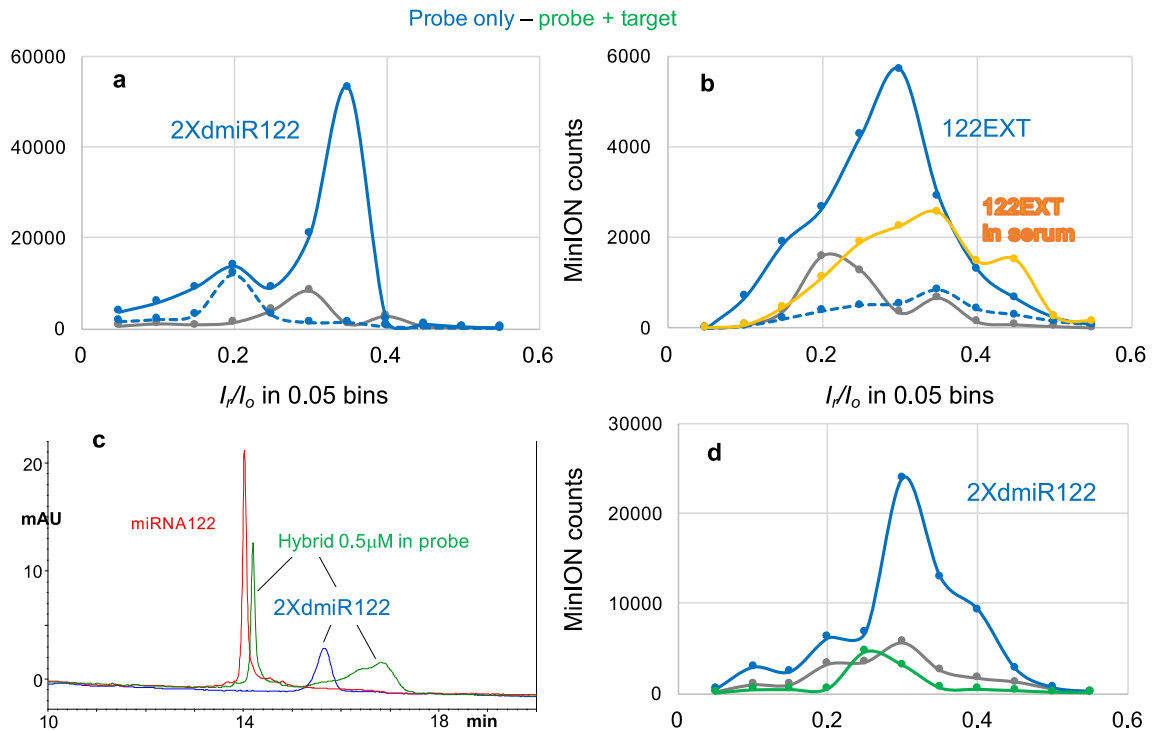


Figure 5. Nanopore experiments testing advanced probe designs and probe detection in 15% human serum—85% ONT buffer. **(a)** Three consecutive nanopore experiments conducted with the same flow cell. (1) Buffer test 0.75 h at -180 mV (grey trace), (2) probe 2XdmiR122 tested 1.5 h at -180 mV (dashed blue trace) and (3) no sample added, voltage raised to -220 mV and experiment run for 1.5 h (solid blue trace). This set of experiments provided solid evidence that, at least, this probe is not traversing the ONT nanopores at -180 mV even during a 1.5 h long experiment. In addition, it illustrated that this probe traverses the pores under applied voltage of -220 mV, and produces a high count of detectable events. **(b)** Four consecutive nanopore experiments conducted with the same but previously used flow cell that carries only around half, i.e. 250, working nanopores. (1) buffer test at -180 mV (grey trace), (2) probe 122EXT at a load 3-times less compared to regular load of 0.38 nmoles tested at -180 mV (dashed blue trace), (3) no sample added, voltage raised to -220 mV (solid blue trace) and (4) new sample with same load of probe 122EXT as in (2), but prepared in 15% human serum—85% ONT buffer (yellow trace). See discussion in text. **(c)** HPLC profiles of (1) intact miRNA122 (red trace), (2) probe 2XdmiR122 at $0.5 \mu\text{M}$, a 10-fold lower concentration compared to our regular $5 \mu\text{M}$ sample concentration (blue trace) and (3) mixture probe to target = 1:2, also at a $0.5 \mu\text{M}$ concentration in probe (hybrid, green trace). All three samples in $>90\%$ ONT buffer and monitored at 260 nm using HPLC method B (see “Experimental section”). The latter two samples were used, as is, for the nanopore experiments shown in **(d)**. **(d)** Consecutive nanopore experiments on the same flow cell. (1) Buffer test, 1 h at -220 mV (grey trace), (2) probe 2XdmiR122, 3 h at -220 mV (blue trace) and (3) hybrid sample with miRNA122, in 2-fold excess over the probe, tested for 1 h at -220 mV (green trace). This experiment confirms sensitivity in the detection of 2XdmiR122, albeit via a 3 h long experiment, and confirms that hybridization with target results in severely reduced counts, i.e. silencing. Data acquisition and analysis for the nanopore experiments as described under Fig. 2a.

General design for a highly detectable probe. The presence of T(OsBp) moieties in the middle of a sequence is not a feature shared by many potential ctDNA or miRNA targets. Therefore, we designed advanced probes by replacing all dTs in the sequence with dU, modifying some or all the bases as 2'-OMe, added 3 adjacent dTs at the 5'-end, and, in some cases added 3 additional dAs at the 3'-end. Addition of dAs at the 3'-end is commonly used to facilitate pore entry^{28–30}. Replacing DNA bases with 2'-OMe bases is known to lead to stronger hybridization⁶⁹. Replacing all dTs within the sequence with dUs assures that the presence of OsBp is minimal within the sequence due to the kinetically higher reactivity of T vs. U or dU towards osmylation (see above). This results in the lowest possible number of OsBp moieties within the sequence and the most unhindered hybridization with the target. The addition of 3 adjacent dTs at the 5'-end makes the probe undetectable at applied voltage of -180 mV and highly detectable at applied voltage of -220 mV, as shown by the earlier experiments with the BJ1-4 probes. We then exploited this probe design in nanopore experiments with extra low target loads.

BJ2 TA(OMe) is a probe designed with the above features (see sequence in Table 1). Hybridization between probe BJ2 TA(OMe) and the complementary primerM13for(-41) was tested by HPLC at the $5 \mu\text{M}$ concentration range (Fig. 4c). Figure 4c presents the HPLC analyses of the probe and of the hybrid samples. The target peak in the hybrid sample is easily identified due to its about 10% excess over the probe. The HPLC profiles at both wavelengths, 272 nm and 312 nm, are shown. Close inspection of these profiles illustrates that the hybrid peak

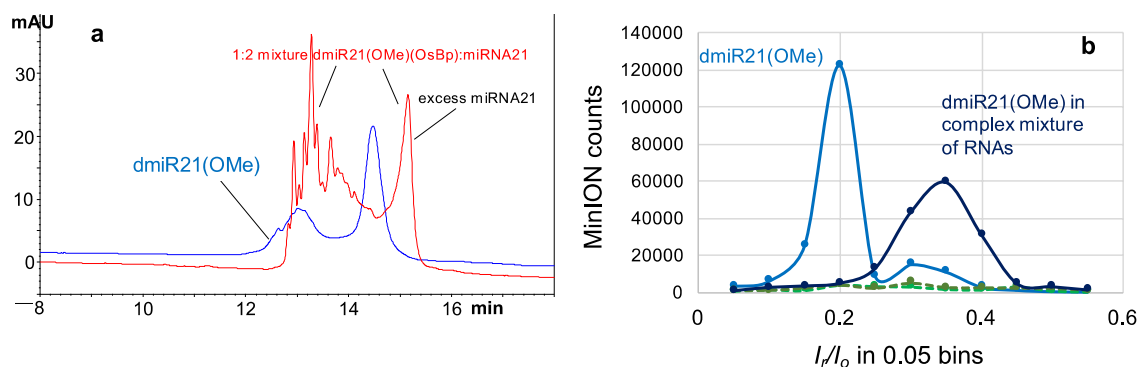


Figure 6. Targeting miRNA21 in a complex mixture. (a) HPLC profiles of two samples analyzed with HPLC method B (see “Experimental section”): (1) probe dmiR21(OMe) at 0.15 nmole load and (2) 1:2 mixture of this probe with miRNA21 at a 0.30 nmole probe load. The probe’s HPLC profile exhibits two peaks, the larger one eluting after the minor one (blue trace). This profile is consistent with the determined value of 2.85 OsBp moieties per molecule, on average, meaning that this preparation includes molecules with 2 and molecules with 3 OsBp tags. The HPLC profile of the 1:2 mixture of probe to target exhibits a single rather sharp peak eluting after a broad rather complex peak (red trace). We confirmed that the sharp peak corresponds to the excess miRNA21 target and attribute the broad complex peak to multiple hybrids, the result of one target and many probes, all complementary to the target, but each one of them carrying OsBp moieties at a different nucleobase. It is reasonable to assume that the chromatography resolves these hybrids, as it resolves topoisomers with such short osmylated oligos⁵⁹ (HPLC method B in “Experimental section”). The observation of distinct HPLC profiles between probe and mixture samples is consistent with hybridization. (b) Four nanopore MinION experiments two of them using the exact samples analyzed by HPLC in (a): (1) probe dmiR21(OMe), tested for 2 h at – 180 mV, exhibited over 100,000 events (light blue solid trace), (2) 1:2 mixture of this probe with miRNA21, tested for 1 h at – 180 mV, exhibited negligible counts (hybrid, light green dashed trace). Two additional experiments tested the effect of excess non-target RNA in the translocation properties of probe dmiR21(OMe) and its hybrid with miRNA21. The excess non-target RNA was at a 10-fold higher load compared to the probe and was composed of equimolar amount of miRNA140 and a 100 nt long RNA. Nanopore experiments in the presence of excess non-target RNA (3) hybrid with miRNA21, 1 h at – 180 mV (dark green dashed trace), and (4) probe dmiR21(OMe), 2 h at – 200 mV (dark blue solid trace). Higher voltage used here to compensate for the hours that this flow cell had worked already, per ONT protocol. The effect of the excess non-target RNA on the hybrid, if any, is not detectable, as the counts are too few. The effect of the excess non-target RNA on the probe appears to be a profile shift and reduced counts by a factor of 2, even though this reduction can be attributed to the number of working nanopores that is also reduced by a factor of about 2. Please note that probe dmiR21(OMe) translocates efficiently at an applied voltage of – 180 mV, as it does not contain any adjacent osmylated dTs. Data acquisition and analysis as described under Fig. 2a.

has about half the contribution at 312 nm, compared to the corresponding contribution in the probe. This is in agreement with the expectation that the hybrid is half probe and half unmodified target. The actual samples tested by HPLC were diluted with ONT buffer to produce the samples tested by nanopore. The protocol followed for this and all dilutions in this study was done by consecutive 1:10 dilutions with ONT buffer in 0.5 mL microcentrifuge tubes. The nanopore experiment with probe BJ2 TA(OMe) was done at a 1000-fold dilution compared to the HPLC sample, i.e. at a 0.38 pmole probe load. The corresponding experiment with the hybrid was conducted at 3.8 pmole, i.e. at a 10-times higher hybrid load. The higher hybrid load was chosen to test the stability of the hybrid under the experimental parameters especially under the influence of the – 220 mV applied voltage. Despite the hybrid sample being 10-times more concentrated than the probe, the counts obtained from the hybrid experiment (green trace) are visibly fewer compared to the counts obtained from the probe experiment (blue trace) and suggest that hybrid dissociation is not significant under the tested conditions (Fig. 4d).

Hybridization silences the probe in the presence of an RNA oligo target. During the development work we experimented with several probe designs. Experiments with two of those designs are illustrated in Fig. 5. Probe 2XdmiR122 is a 44 nt oligo with 8 T(OsBp) and consists of two fused dmiR122 (see sequence in Table 1). Even though probe dmiR122 exhibited numerous counts at – 190 mV (Fig. 2b), probe 2XdmiR122 required – 220 mV (Fig. 5a). The higher voltage is most likely the consequence of heavy crowding within the pore, as 2XdmiR122 incorporates two 4 nt groups with 3 OsBp each within a subsequence of 26 nt. Efficient hybridization between miRNA122 and 2XdmiR122 was shown by HPLC (Fig. 5c) and confirmed by nanopore, as seen by the huge drop of counts for the hybrid sample (green trace) compared to the probe sample (blue trace, Fig. 5d). The advantage of such fused sequence design lies in exploiting cases where the identical sequence of bases is present in a longer RNA in addition to a miRNA target. Using a probe with a design like the fused 2XdmiR122 may favor hybridization with the miRNA target over the long RNA target, as 2XdmiR122 can form a 44 nt ds complex with miRNA122, but only a 22 nt ds complex with the longer RNA.

Figure 5b presents an additional probe design, exemplified by probe 122EXT (sequence in Table 1). Probe 122EXT has the identical sequence of dmiR122 with the addition of 3 adjacent dTs at the 5'-end. This probe

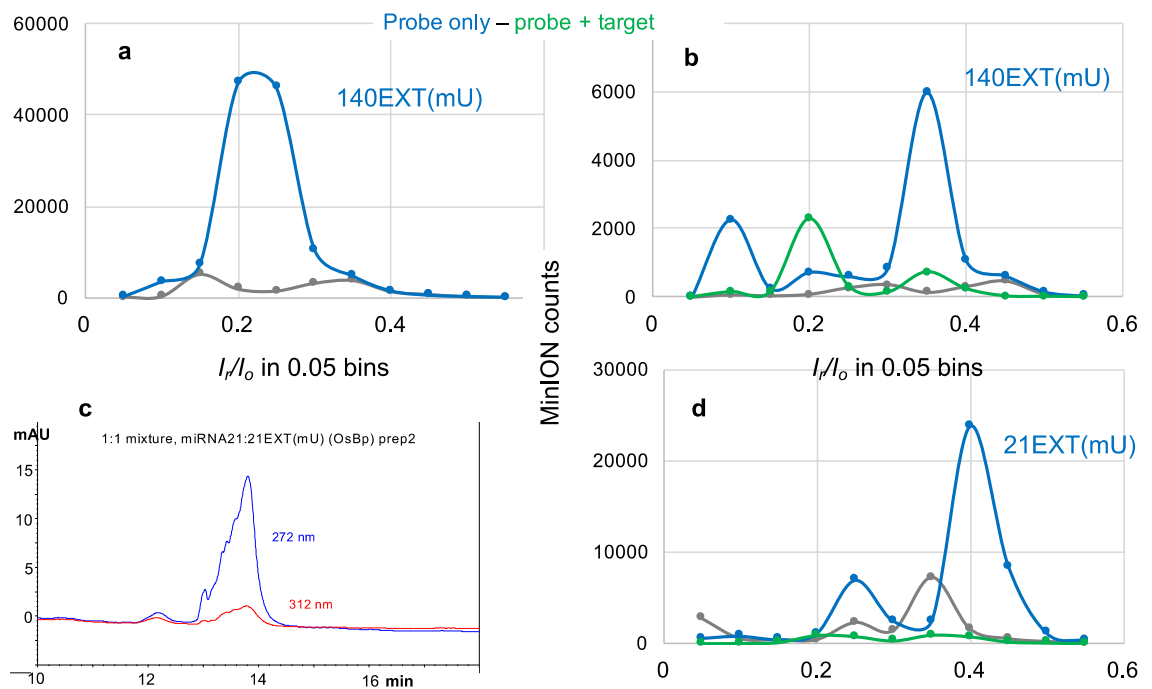


Figure 7. Nanopore experiments targeting miRNA140 or miRNA21 at single-digit attomole load. (a) Consecutive nanopore experiments conducted with the same flow cell: (1) buffer test, 1 h at -210 mV (grey trace), (2) probe 140EXT(mU) at a 47 fmole load, 1.5 h at -210 mV. (b) Consecutive nanopore experiments conducted with the same used flow cell with less than 200 working nanopores: (1) buffer test, 1 h at -210 mV (grey trace), (2) probe 140EXT(mU) at a 3.5 amole load, 1.5 h at -210 mV (blue trace) and (3) equimolar mixture of 140EXT(mU) and miRNA140, at 3.5 amole load each, 1.5 h at -210 mV (hybrid, green trace). (c) HPLC profile of a sample with equimolar concentration of probe 21EXT(mU) and target miRNA21 using HPLC method B (“Experimental section”). The appearance of a single peak is consistent with hybridization. Sample monitored at two different wavelengths to show the absorbance at 312 nm attributed to the presence of the osmylated probe. (d) Consecutive nanopore experiments with the same flow cell; samples were first tested by HPLC, then diluted with ONT buffer by a factor of 10^9 or 3×10^8 for probe or hybrid, respectively (see text and “Experimental section”). (1) buffer test, (grey trace), (2) probe 21EX(mU) at 0.9 amole, (blue trace), and (3) 1:1 mixture of probe 21EXT(mU) with miRNA21 at 2.8 amole load each, (hybrid, green trace). Hybrid exhibits dramatically fewer counts compared to the probe. Data acquisition and analysis for the nanopore experiments as described under Fig. 2a.

requires -220 mV to show numerous counts (blue solid trace), as seen by comparison to the nanopore experiment at -180 mV (dashed blue trace). A nanopore experiment conducted with probe 122EXT in a sample prepared in 15% human serum and 85% ONT buffer (yellow trace) exhibits about half the counts compared to the sample prepared in over 95% ONT buffer (blue solid trace). The reduction in counts may be attributed to the lower ionic strength due to the presence of serum, and/or to the aged flow cell and/or to serum interference. Despite the lower counts probe 122EXT is easily discriminated from the control/buffer test (grey trace) indicating the unhindered probe detection in an unknown sample that contains a body fluid, such as human serum.

miRNA21 is an important biomarker for a number of diseases^{64–68}, so its identification was our priority. HPLC tests with miRNA21 and probes dmiR21, or 21EXT indicated no detectable hybridization with miRNA21 (Fig. S6 in the Supplementary Information). Inability to form the hybrid was attributed to the presence of more than 5 T(OsBp) moieties and the fact that these moieties are spread over the 22 nt sequence. Advanced probe design led to probes that efficiently hybridized with miRNA21. Probe dmiR21(OMe) is a 22 nt oligo, complementary to miRNA21, where all bases are 2'-OMe, dTs are replaced with mU, and osmylation resulted in the addition of 2.85 OsBp moieties, on average, per molecule (see Table 1 and “Experimental section”). Please note that mU is 2'-OMe-U and 2'-OMe-base-deoxyribose is the same chemical as 2'-OMe-base-ribose. The osmylated product is a mixture containing primarily molecules with 2 or 3 OsBp moieties, and also molecules containing OsBp moieties at different bases (called here topoisomers)^{49,58}. Our chromatography resolves molecules that carry one, two or three OsBp moieties and often resolves topoisomers too⁵⁹. This is why the HPLC profile of the probe consists of two separate peaks attributed to a molecule with 2 tags and to a molecule with 3 tags (blue trace, Fig. 6a). Similarly, the HPLC profile of the hybrid appears as multiple peaks (red trace, Fig. 6a). We tested by HPLC the stability of RNAs (see below) and the stability of the hybrid of probe dmiR21(OMe) with miRNA21 in a solvent composed of 15% human serum and 85% ONT buffer. Fig. S7b illustrates that the tested RNAs, i.e. miRNA140 and the 100 nt RNA, both degraded within minutes, whereas the hybrid peak remained practically unchanged, suggesting that the hybrids formed between our probes and their RNA targets are expected to be stable during the duration of a nanopore experiment in human serum/ONT buffer.

Hybridization is consistent with the distinct HPLC profiles observed with the probe and the hybrid samples (Fig. 6a). Because dmiR21(OMe) does not contain 3 adjacent T(OsBp), applied voltage at -180 mV was sufficient to thread this probe via the pore. Plenty of events were reported with a 0.75 nmole probe sample and markedly fewer with a 1.5 nmole hybrid sample (Fig. 6b, compare solid light blue trace with dashed light blue trace). Counts with the hybrid (19,647) are comparable to the counts obtained from the buffer (7680) and markedly lower compared to the probe (194,810). Two additional nanopore experiments were conducted with the same probe and hybrid loads, as before, but in the presence of excess non-target RNA components. These components were miRNA140, and a 100 nt RNA, at a total 10 -fold higher load compared to the probe. The nanopore profiles of the probe samples with or without the excess non-target RNA are distinct suggesting influence by the excess material and/or an aged flow cell (light blue vs. dark blue solid traces). Still the two experiments in the presence of the non-target RNA show efficient identification of the target by comparing the numerous counts of the probe sample (dark blue solid trace) to the few counts of the hybrid sample (dark blue dashed trace). This discrimination suggests that the presence of non-target miRNAs and longer RNAs in a complex mixture do not prevent target identification.

Due to the importance of miRNAs as biomarkers^{63–68}. We conducted experiments at extra low load with a probe design that is broadly applicable to any target sequence and exhibits optimal translocation properties. We selected probes 140EXTmU and 21EXTmU (see sequences in Table 1) to target miRNA140 and miRNA21, respectively. These probes have a sequence complementary to their target, mU replacing T within the sequence, 3 additional adjacent dTs at the 5'-end, and 2 or 3 additional dAs at the 3'-end. These oligos were osmlyated using the validated labeling process that adds, on average, 4–5 OsBp tags per molecule, 3 of which occupy the 5'-end, and the other 1 or 2 are randomly allocated within the sequence (see Table 1 and “Experimental section”). Due to the heavy crowding at the one end of the probe, applied voltage in the range of -210 ± 10 mV is required for probe efficient translocation and detection (see discussion above). Figure 7a illustrates detection with excellent sensitivity at the 47 fmole level with 140EXT(mU), and Fig. 7b illustrates detection of this probe at an even higher sensitivity of 3.5 amole probe load. Identification of the target miRNA140 is also evident by comparing the probe (blue trace) to the hybrid (green trace) with hybrid load also at 3.5 amole. Figure 7c shows the HPLC profile of the hybrid sample between probe 21EXT(mU) and miRNA21, which was then diluted by a 3×10^8 factor for the nanopore experiment to test the hybrid at the 2.7 amole level (green trace in Fig. 7d). The 21EXT(mU) probe sample [HPLC profile included in Fig. S14 (Supplementary Information)] was diluted by a 1×10^9 factor in order to conduct the nanopore experiment at the 0.9 amole level of (blue trace in Fig. 7d) which is the lowest load tested in this study. Identification of miRNA21 is evident in Fig. 7b by visual comparison of the numerous probe counts (blue trace) to the few counts of the hybrid (green trace). The reason that the counts observed with the 140EXT(mU) probe (top reaching 6000) are fewer compared to the counts observed with the 21EXT(mU) probe (top reaching 24,000) is, at least partially, due to an aged flow cell that had only about 30% of working pores. Whether or not proportionality in probe counts can be obtained from the ONT/OsBp platform for a specific probe was not tested here, primarily because probe concentration is a known quantity. Most importantly, identification of the target is based on a nanopore profile that exhibits an insignificant number of counts, also comparable to the counts of the control/buffer experiment. The main reason we tested every probe by nanopore, is because we wanted to compare different probe designs and confirm high detectability and high sensitivity.

The potential of the ONT/OsBp nanopore platform. The above experiments range in probe load from 0.38 nmole to 0.9 amole, practically spanning 9 orders of magnitude. In this range evidence is presented for probe detection, and clear distinction between the sample that contains the target and the sample that does not. We propose as lower detectability limit, 3-times higher count of events with probe alone compared to the counts of the hybrid. Proportionality between the count of events and the probe concentration was not tested here, as the duration of the experiments remains in the range of 1–3 h and does not reflect the sample load variation. Since our test does not detect the hybrid and therefore does not measure the hybrid molecules, quantification of the target depends on the known probe load. The test requires an estimate for target load and depending on the outcome of the first experiment, one can vary the probe load by a factor of 5 below or above in the next experiment. We estimate that target quantification can be attained with about 30% accuracy. Here we explored a number of probe designs and proposed one design that can practically match any ssDNA or ssRNA oligo target. This type of probe, with examples identified as 140EXT(mU) and 21EXT(mU), exhibited high sensitivity at the amole load level. No attempt was made to test for specificity. Discrimination between one target and another target with similar sequence will need to be addressed case-by-case. The HPLC method developed here can evaluate hybridization between a target and a tentative probe and it can also assess probe hybridization extent and tentative discrimination between two targets with similar sequence. Here the flow cell temperature was at the factory preset temperature, but nanopore proteins are known to be stable in a certain temperature range. Flow cell temperature, if left at the discretion of the user, can provide a means to improve specificity. We also did not replace the proprietary ONT Flush buffer. The latter was developed for sequencing, and a different buffer may be more suitable for our application.

Preliminary experiments indicate that the hybrid of miRNA21 with dmiR21(OMe) is relatively stable in a 15–85% serum-ONT buffer and that probe 122EXT is detectable by nanopore in a 15–85% serum-ONT buffer. These experiments suggest that using the ONT/OsBp nanopore platform with blood serum samples is feasible. Considering that the MinION flow cell uses 75 μ L sample volume and 15% could be blood serum, then approximately 11 μ L of a human serum sample can be directly tested in a nanopore experiment. Assuming that an 11 μ L human serum sample contains about 3 amole of miRNA21, miRNA140, or tentatively any other miRNA, our

general probe design should be able to detect it, and as a corollary detect the presence/absence of the target. In this context, our test qualifies as a follow-up, point-of-care diagnostic test.

Even though not tested here, RNA-based probes may successfully target a relatively short dsDNA after addition of the probe to the unknown sample and denaturation. Such identification may be feasible, as RNA/DNA hybrids are known to be more stable compared to DNA/DNA hybrids. RNA probes exhibit a different nanopore profile compared to DNA-based probes, as indicated by comparison of the $(I_r/I_o)_{\max}$ in Fig. 2a with the corresponding $(I_r/I_o)_{\max}$ in all the other figures representing probes. This feature can lead to probe multiplexing in order to test more than one target at a time. Similarly, probes like dmiR21(OMe) that are missing the 3 adjacent dTs at the 5'-end were seen to translocate at -180 mV, while probes with 3 adjacent dTs require -220 mV. This distinction may be also exploited in order to multiplex probes. Distinct nanopore profiles will reveal which one of the probes is silenced. With just one probe, the test can conclusively identify the presence/absence of the target by comparing the total count of events of the probe alone to the total count of events of the mixture of the probe with the unknown sample. With a multiplexed test, counts should be plotted as histograms, just as presented here, in order to determine which probe is missing.

Conclusions

We presented ion-channel single molecule experiments conducted using portable, commercially available nanopore devices from ONT. While a number of experimental nanopore platforms paved the way for using nanopores as single molecule sensors, our work appears to be the first to explore ONT devices. The proposed test targets DNA and RNA oligos and exhibits a 9 orders of magnitude range of detection, approaching single-digit attomole target sensitivity from an 11 μ L sample. Our technology exploits the relatively slow data acquisition rate of the ONT platform in which native oligos traverse through the nanopores too rapidly to be detected, while probes selectively tagged with a bulky Osmium label (OsBp) traverse at a slower, detectable rate. Furthermore, OsBp modified probes hybridized to a target oligo do not enter the pore, effectively “silencing” the probe by quantitatively reducing the number of detected events. This silencing allows quantification of the target based on the known concentration of the probe. These properties enable detection and quantification of highly dilute samples such as ctDNA and miRNAs found in bodily fluids.

Expense and product quality considerations led us to select DNA over RNA oligos as probes. Our experiments revolved around optimizing the probe's design to make it of general applicability, and aptly detectable by the proprietary ONT/CsGg nanopore. A probe that successfully identified miRNA targets at the single-digit attomole level has sequence complementary to the target, 2'-OMe-U replacing dT within the sequence, 3 additional adjacent dT residues at the 5'-end, and 3 added dA residues at the 3'-end. Additionally, the oligo is osmylated to add 4–5 OsBp tags per molecule, 3 of which occupy the 5'-end, and the other 1 or 2 are randomly allocated within the sequence. Due to the heavy crowding at the one end of the probe, applied voltage in the range of -210 ± 10 mV is required for probe translocation and detection. This feature is advantageous, as it allows for depletion of non-target material at -180 mV prior to performing the diagnostic experiment at -210 mV. Probes may also be multiplexed and target up to 3 oligos when using probe designs that exhibit distinct nanopore profiles. Preliminary experiments in 15% human serum suggest that probes and the resulting hybrids are stable in such medium, and show the feasibility for identifying short DNA and RNA from body fluid samples using the ONT/OsBp nanopore platform.

Experimental section

RNAs and other reagents. Custom-made RNA oligos were purchased from Dharmacon (Horizon Discovery Group). Custom-made deoxyoligos were purchased from Integrated DNA Technologies (IDT). Circular ssM13mp18 was purchased from Bayou Labs, and osmylated at Yenos Analytical (see Table S1 in the Supplementary Information). Sequences and UV/Vis properties of their osmylated derivatives are listed in Table 1. Purity of oligos was tested by HPLC in-house and typically found to be $>85\%$. Oligos were diluted with Ambion Nuclease-free water, not DEPC treated, from Thermo Fisher Scientific typically to 100 or 200 μ M stock solutions and stored at -20 °C. HPLC profiles from the analyses of both the intact and the osmylated oligo are included in the Supplementary Section. Buffer DNase-free and RNase-free TRIS.HCl 1.0 M pH 8.0 Ultrapure was purchased from Invitrogen and used to prepare the HPLC mobile phase. NaCl crystalline ACS min 99.0% from Alfa Aesar. Distilled water from Alhambra was used for preparation of HPLC mobile phase. A 4% aqueous osmium tetroxide solution (0.1575 M OsO₄ in ampules at 2 mL each) was purchased from Electron Microscopy Sciences. 2,2'-Bipyridine 99+ % (bipy) was purchased from Acros Organics. Human Serum from human male AB plasma and NaOH 1 N Bioreagent were purchased from Sigma. ssM13mp18, primer M13(fwd6097), NEBuffer 2.1, and Klenow Fragment of DNA Polymerase I (3'-5' exo)(M0212) were kindly provided by New England Biolabs, Ipswich, MA, USA.

(Pyrimidine)OsBp is a chromophore. Selective labeling of a nucleic acid requires an assay for quality control. Addition of OsBp to the C5-C6 Py double bond and formation of Py(OsBp) creates a new chromophore in the wavelength range of 300 to 320 nm⁵⁴, where nucleic acids exhibit negligible absorbance. We exploited this observation and used a deoxyoligo training set to show that extent of osmylation can be measured using the equation: $R(312/272) = 2 \times (\text{No of osmylated pyrimidines}/\text{total nt of nucleotides})$ ⁵⁴. Value $R(312/272)$ is the ratio of the observed peak absorbance at 312 nm over the observed peak absorbance at 272 nm (the peak shape could be sharp or broad or multiple peaks)^{54,58,59}. The wavelengths 312 nm and 272 nm were chosen in order to maximize the effect and to equalize contributions by different pyrimidines⁵⁴. Absorbance at 272 nm is about 75% of the absorbance at 260 nm practically for either intact or osmylated nucleic acids. Using the ratio R instead of the absorbance at 312 nm normalizes the measurement, and minimizes instrument sampling variation.

As deduced by experimenting with an oligo training set, when observed value $R(312/272) = 2 \times$ (# of pyrimidines/total # of nucleotides), osmylation is practically 100% complete and all the pyrimidines carry one OsBp moiety^{54,58}. When observed $R(312/272) < 2 \times$ (# of pyrimidines/total # of nucleotides), osmylation is partial and the number of osmylated pyrimidines or OsBp moieties can be calculated based on the same equation (see columns # 5 and 7 in Table 1). With partial osmylation the number obtained from the equation refers to OsBp moieties, on average. Molecules carry an integer number of OsBp moieties and therefore some molecules will have fewer, and some molecules will have more than the calculated value distributed in a statistically unbiased manner. We have shown that osmylation occurs randomly, but depends on the relative reactivity of OsBp for the pyrimidines. Relative reactivity towards osmylation, determined by kinetic measurements at 26 °C in water using deoxyribooligos⁴⁴ is $T/dC = 28$, $dU/dC = 3.75$ and therefore $T/dU = 7.5$, in agreement with earlier studies⁵⁸. Comparable kinetic measurements of OsBp reactivity towards ribooligos determined $U/C = 4.7$ and $5\text{-MeU}/C = 44$ ⁴⁹; hence $5\text{-MeU}/U = 9.3$, with 5-MeU carrying the identical nucleobase as T. These measurements suggest that reactivity of OsBp towards a nucleotide is primarily determined by the identity of the nucleobase, while the sugar and the backbone make an insignificant contribution. Because of the markedly higher reactivity of OsBp towards T, compared to U and C, conditions can be found to osmylate practically 100% all dTs, while some dU and very few dC become osmylated^{54,58}. We have exploited this dramatically higher reactivity, added 3 dTs at the 5' end of a probe, replaced the dTs in the sequence with dU or mU, in order to keep the base-pairing with Adenosine in the target intact, and optimized the manufacturing process as detailed below.

Manufacturing of OsBp-nucleic acids. OsBp reagent is prepared by weighing the equivalent of 15.7 mM of bipy (49.2 mg) in a 20 mL scintillation vial, adding 18 mL of water and stirring at room temperature until bipy dissolves, followed by transferring the full content of a 2 mL 4% OsO₄ solution supplied in an ampule. Dissolving bipy in water before the addition of OsO₄ (protocols a, b, c, and d) results in a more consistent and potent preparation compared to dissolving bipy after the addition of OsO₄ (protocol o). The transfer should be done using a glass pipette inside a safety hood⁷⁰. The resulting solution is an aqueous 20 mL 15.75 mM OsBp (0.4%) stock solution, equimolar in OsO₄ and bipy. The concentration of the OsBp stock solution is limited by the solubility of bipy in water and adding OsO₄ does not increase it, as the complex has a low association constant. OsBp complex represents an approximate 5% of the total, as measured by CE⁵⁸. Care should be taken that this preparation, as well as any other work using OsBp is conducted in stoppered glass vials in a well-ventilated area. Leftover solutions of OsO₄ and/or OsBp may be mixed with corn oil to neutralize unreacted OsO₄ and properly discarded based on specific local regulations⁷⁰. The freshly prepared OsBp stock solution is dispensed in HPLC vials and kept at -20 °C. Each vial can be stored at 4 °C and used for a month without loss of potency; typical pipette tips can be used for manufacturing of OsBp-labeled nucleic acids. OsBp stock solutions should be validated before first use by running a known reaction. For osmylation reactions a 20-fold excess of OsBp over the reactive pyrimidine in monomer equivalents is required to ensure pseudo-first order kinetics, and to assure successful use of protocols. Manufacturing conditions, i.e. OsBp concentration and labeling duration varies significantly depending on the presence of T, and the desired result of osmylating all pyrimidines, T only, or just a fraction of C and U in RNA. For the purpose of this study, when T-osmylation is required protocol b is recommended and when partial osmylation of U and C is required protocol c is recommended. These choices were facilitated by testing additional protocols (o and a), as identified in Table 1. Protocol d is used when the probe carries no Ts. Quenching of the osmylation reaction occurs upon purification. Purification from excess OsBp was done with spin columns (TC-100 FC from TrimGen Corporation) according to the manufacturer's instructions. Briefly, spin columns are filled with the manufacturer's proprietary solution and centrifuged at 4000 rpm for 4 min; the resulting solution and the microcentrifuge tube are discarded. Then 40–120 µL of an osmylation reaction mixture is transferred to the spin column and centrifuged at 4000 rpm for 4 min using a clean microcentrifuge tube. The centrifuged solution is the purified osmylated oligo. This purification method retains the volume/concentration of the sample, and close to 100% recovery of RNA is achieved. For purity and characterization of the intact and osmylated oligos see Figures S8–S18 in the Supplementary Information.

Recommended protocol b for T-osmylation is 30 ± 2 min incubation with 2.6 mM OsBp in water at room temperature (see Table 1 under ^b). Recommended protocol c for partial U- and C-osmylation of probes that do not carry dTs is 30 ± 2 min with 3.9 mM OsBp in water at room temperature (see Table 1 under ^c). There were two additional protocols tested, but found to be less optimal: protocol where bipy was not dissolved in water prior to the OsO₄ addition and used 40 min incubation with 2.6 mM OsBp (see Table 1 under ^o) and the protocol using 45 min incubation with 2.6 mM OsBp (see Table 1 under ^a). The presence of 2'-OMe groups does not affect markedly the extent of osmylation, as seen by comparable osmylation extent for 100 nt RNA and 100 nt RNA(2'-OMe) that carries about 50% 2'-OMe bases. What affects osmylation extent is the number of U in the oligo as seen in Table S2 and Fig. S19 in the Supplementary Information. This is because the reactivity of OsBp towards U is 4.7 times higher compared to the reactivity towards C. Because the osmylation protocols do not go to completion U(OsBp) or mU(OsBp) are kinetically preferred over C(OsBp). With protocol^b osmylation of other pyrimidines is negligible compared to T-osmylation, but with protocol^c the extent of osmylation towards U and C is measurable (Table S2 in the Supplementary Information). Fig. S19 suggests a linear correlation between the number of OsBp moieties and the number of U present in an oligo spanning from 22 to 100 nt oligos. One may use the slope = 0.43 of the graph to estimate extent of osmylation with protocol^c for any oligo based on the number of Us in the sequence.

We used 2 mL HPLC vials fitted with 120 µL glass inserts to carry the manufacturing reactions. Removing the reaction product from these inserts and transferring it onto the purification spin column requires a long and narrow 20 µL pipette tip. Osmylated nucleic acids are as stable as the corresponding nucleic acid, and the OsBp label is unreactive. They can be stored in the 1.5 mL microcentrifuge tubes, at -20 °C for years. The

concentrations of 2.6, 3.9 and 5.2 mM correspond to 1/6, 1/4 and 1/3 dilutions of the 15.75 mM OsBp stock solution, respectively. Deviations from these two protocols are included in Table 1, identified as protocols ^o and ^a. An additional protocol (^d) was used in order to achieve higher extent of osmylation with probes that do not contain any T, such as dmiR21(OMe) and make it a detectable probe.

Enzymatic elongation reactions. The ability of DNA polymerase to extend an osmylated primer was examined in vitro using ssM13mp18 annealed to unmodified and osmylated oligonucleotides. ssM13mp18 at a concentration of 42 nM was mixed with 0.42 μ M primer in NEBuffer 2.1 (New England Biolabs). Samples were heated to 90 °C for 30 s and cooled to 25 °C at 0.1 °C/s. Polymerization reactions contained these annealed complexes: 8.4 nM M13mp18, 1.25X NEBuffer 2.1 (NEBuffer is 10 mM TrisHCl pH 7.5, 50 mM NaCl, 1 mM EDTA), 0.25 mM each of dGTP, dATP, and dTTP, 0.025 mM α -[³²P] dCTP, and 7 U/mL Klenow Fragment of DNA Polymerase I (3'-5' exo-) (NEB, M0212). Reactions were incubated at 37 °C and incorporation of labeled dCMP was monitored by an acid precipitation assay. Time points were taken at 5, 10, and 20 min.

As seen in Fig. 3a, no incorporation was noted when no oligonucleotide was added, or if the oligonucleotide, primerM13rev(-48), was not complementary to the ssM13mp18. In contrast, most oligonucleotides predicted to anneal to the DNA template gave robust incorporation, even when osmylated, with maximal incorporation corresponding to roughly one round of replication on the M13mp18 DNA template. Incorporation noted for M13(fwd6097), BJ2, BJ3, and BJ4 were equivalent despite interior single base mismatches within BJ3 and BJ4 (see sequences in Table 1). Despite overall equivalent osmylation levels for BJ2, BJ3 and BJ4, markedly lower levels of incorporation were noted for BJ1, most likely due to presence of OsBp at the terminal 3'-T(OsBp) residue.

HPLC methods. The HPLC method to assess oligo purity was developed earlier, and used here to assess purity of the oligos listed in Table 1. This method was optimized (see below) and used to assess hybridization between two oligos in a mixture; validation of this method was conducted using a 1:1 mixture of intact oligos known to hybridize (see Fig. 3b). Analyses were conducted automatically using a thermostatted autosampler. HPLC peaks were detected and identified using a diode array detector (DAD) in the UV-Vis region 200–450 nm. The chromatograms were recorded at 260, 272, and 312 nm and reported here selectively. Samples were prepared with RNase free water, but buffers were not.

For HPLC analysis we used an Agilent 1100/1200 LC HPLC equipped with a binary pump, Diode Array Detector (DAD), a 1290 Infinity Autosampler/Thermostat, and Chemstation software Rev.B.04.01 SP1 for data acquisition and processing. For sample analyses we used IEX HPLC column DNAPac PA200 from ThermoFisher Scientific (Dionex) in a 2 \times 250mm configuration. The performance of the instrument and the column was qualified using standards every time ahead as well as after analysis of research samples. The HPLC method was developed to assess hybridization in a sample approximately 90% in aqueous ONT buffer at pH 8 and column thermostat at 35 °C. This HPLC method (identified as B) uses the DNAPac PA200 column with a 0.45 mL/min flow, mobile phase A (MPA) aqueous 25 mM TRIS.HCl pH 8 buffer, mobile phase B (MPB) aqueous 1.5 M NaCl in a 25 mM TRIS.HCl pH 8 buffer, a gradient from 10% MPB to 50% MPB in 20 min and an additional 10 min for wash and equilibration to initial conditions, i.e. 90% MPA. Column temperature was set at 35 °C to mimic the flow cell temperature. To include the 100 nt RNA the chromatography was modified to HPLC Method C. Specifically the gradient was made steeper, 10% MPB to 75% MPB in 20 min, and everything else remained as is. Because of the approximately neutral pH the long 100 nt RNA elutes as a broad peak resembling a mixture. This is because aqueous pH 8 does not denature the various conformations of a long RNA, as reported earlier⁶¹. ONT buffer is proprietary material, and its composition is not known to us. ONT buffer has a UV-Vis component that in this chromatography elutes in the void volume and does not interfere with the analysis of the samples. Sample injection volume was typically at 5 μ L, and not higher than 10 μ L. Please note that for the hybridization test to work this chromatography should be used in conjunction with samples in ONT buffer or any other medium that favors complexation. Some of the oligos and their osmylated derivatives were analyzed using a method identified as HPLC method A, which is recommended for oligo purity analysis⁶¹, but not suitable to test hybridization. HPLC method A uses the DNAPac PA200 column with a 0.45 mL/min flow, and column temperature at 30 °C. Mobile phase A (MPA) aqueous pH 12.0 \pm 0.2 with 0.01 N NaOH, mobile phase B (MPB) aqueous 1.5 M NaCl in pH 12.0 \pm 0.2 with 0.01 N NaOH, a gradient from 20% MPB to 95% MPB in 12 min and an additional 8 min for wash and equilibration to initial conditions, i.e. 80% MPA.

Single molecule ion-channel conductance experiments with the CsGg nanopore in a MinION or a Flongle (ONT platform). ONT instructions were followed, as needed. Briefly, a new flow cell is flushed with ONT Flush buffer via the priming port in order to remove the storage solution. The sample is added via the sample port, while the priming port is open. Air bubbles from the flow cell are removed from the priming port right before every use. We stored the flow cells in ONT Flush buffer for up to 2 months, while using them as needed. The MinION takes a 75 μ L sample and the Flongle a 30 μ L sample. Flongle flow cells require an adaptor but work on the same device as the MinION flow cells. The software MINKNOW to run the nanopore experiments was downloaded on a MacBook Pro laptop used for these experiments. All the functions necessary to test the flow cell and run the experiments are done via the MINKNOW software tool. Raw data files were acquired in *fast-5* format, which were then analyzed by the *OsBp_detect* software. Size of *fast-5* files for the experiments depend on the flow cell and experiment duration and vary between 1.5 and 6 GB. *Fast-5* files can be directly visualized in MatLab (from Mathworks) 2D format, once the experiment is completed. MINKNOW allows for monitoring in real time any chosen channel, up to 10 channels, so one does not need to wait for the experiment to be done to see the *i-t* recordings.

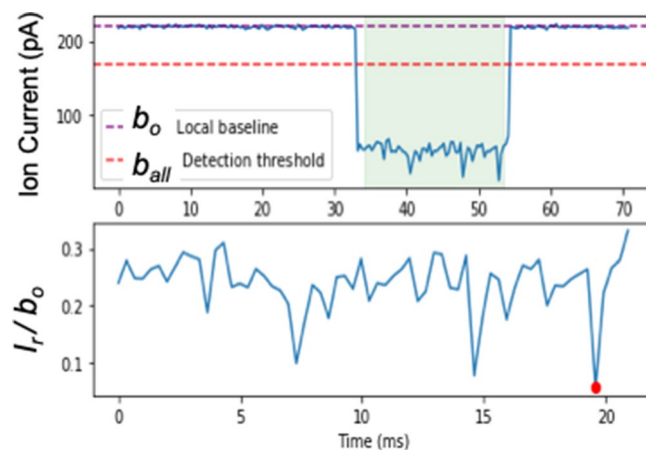


Figure 8. Stages of the event detection pipeline. Top: following the estimation of the baseline open current, b_o , outlined in purple, candidate events that cross the detection threshold, b_{all} outlined in purple, are identified and highlighted in green. Bottom: the identified event is accepted if it satisfies the event duration and $\min(I_r/b_o)$ thresholds. The $\min(I_r/b_o)$ value is highlighted in red.

Samples were either intact oligos or Zenos proprietary osmlyated RNA oligos, or mixtures thereof. Concentrations were typically at or below 10 μM oligo in no less than 80% of ONT buffer. No library was prepared, and no processing enzyme was added, such that all the translocations reported here are unassisted and voltage-driven. Experiments lasted no longer than 1.5 h, but the same experiment could be extended by stopping it, and restarting it later, or next day without adding a new sample. Running more than 2 experiments per day on the same flow cell was avoided. In most cases the first experiment was a “buffer or control test” to assess the flow cell’s baseline. We were surprised on how many events are produced by the ONT buffer and anticipate that ONT may be able to recommend a more suitable buffer for our applications. Duration of the buffer test was kept as short as possible, because the nanopores do not last for more than 15 h under our experimental conditions. Per ONT protocol, applied voltage was raised by about 10 mV for every 5 working hours, in an attempt to keep the open pore ionic current (I_o) constant. This is why experiments compared to one another are done at seemingly different applied voltage. The MinION flow cell has over 2000 nanopores, but only 512 are monitored simultaneously. During the first few experiments on a flow cell, nanopores become inactive, but they are replaced with new working ones. Therefore, the first 4–5 experiments are practically done with the same number of pores. After that the number of working nanopores decreases by 5–10% per hour. It is worth noting that while most of the working nanopores exhibited comparable number of events within a factor of 5 from lowest to highest, a small percentage deviated and recorded markedly higher count of events. We attribute the occurrence of outliers to sample inhomogeneity within the microfluidics of a flow cell and/or to plausible differences within the same batch of protein nanopores, making a small percent of them highly conducive to translocation events. We call these pores “outliers” and found an approximate 2.5% of nanopores to be outliers. The analysis of the data we presented here includes the recordings from all channels including the recordings from the outliers. We performed an additional analysis of all the experiments by excluding the outliers, and even though the actual counts were less, the trends and conclusions are identical to the ones presented here.

Event detection algorithm—OsBp_detect. Let y be an ordered sequence of real values representing a typical time-series obtained from a single Nanopore. We categorize regions of y into one of two states: current from an open channel, I_o , where the Nanopore is unoccupied, and the residual current when some translocation event is taking place, I_r . For the high-throughput characterization of a single translocation event corresponding to an OsBp-tagged oligonucleotide, we propose a segmentation algorithm that can determine the start and end positions in y for all events of interest based on user-defined thresholds. The analysis pipeline is divided into three steps:

1. Baseline current estimation
2. Identification of potential candidate events
3. Event filtering based on event features

First, the baseline I_o , b_o , is established by taking a median of the signal values between estimated lower and upper bounds, $\{o_{low}, o_{up}\}$, of the open current: $b_o = \text{med}(\{i : i \in y, o_{low} < i < o_{up}\})$.

While the signal noise is dependent on the Nanopore platform used, the sharp transitions between the I_o and I_r states from osmium-tagged oligos permit the use of a single threshold-based parser for event detection pipeline. With this approach, events are identified if they pass a set threshold away from the local baseline level. The threshold is defined by parameter b_{all} which should be low enough to capture as many translocation events as possible (Fig. 8). By default, $b_{all} = b_o \cdot (1 - \frac{10 \cdot \sigma_o}{b_o})$ where σ_o represents the signal noise of the open current.

The noise constant, σ_o , is determined by splitting y into small segments (segment size used, $n = 100,000$) and calculating the global standard deviation of the open current signal values, $\sigma(\{i : i \in y, o_{low} < i < o_{up}\})$. The σ_o value additionally provides a useful quality control metric to detect pores with unstable baselines and large events rates or pores that have been blocked.

Finally, for the qualification of valid translocation events, we apply two filtering conditions to the identified events. The filters correspond to the minimum and maximum event length defined by parameters, $\{t_{min}, t_{max}\}$, and the range of lowest residual current, $\{b_{min}, b_{max}\}$, expressed as a ratio with respect to b_o . The event length thresholds, $\{t_{min}, t_{max}\}$, can be adjusted to monitor the speed of translocation whereas $\{b_{min}, b_{max}\}$ enables the separation of OsBp-tagged and untagged oligo species. Let τ_1 and τ_2 represent the starting and ending indices for any given event in y . For $y_{\tau_1:\tau_2}$ to be classified as a potential OsBp translocation event, both of the following conditions must hold:

$$\begin{aligned} t_{min} &< \tau_2 - \tau_1 < t_{max} \\ b_{min} &< \frac{\min(y_{\tau_1:\tau_2})}{b_o} < b_{max} \end{aligned}$$

The event detection pipeline is available as a Python library, 'osbp_detect'. A cross-platform graphical user interface has been included, to enable direct reporting of translocation events from ONT bulk *fast5* files (https://github.com/kangaroo96/osbp_detect).

Data availability

All of the data generated during this study are included in this published article (and its Supplementary Information files). All of raw *i-t* data (each file is 2–6 GB) may be obtained by request from AK.

Received: 1 October 2020; Accepted: 28 October 2020

Published online: 13 November 2020

References

- Bronkhorst, A. J., Ungerer, V. & Holdenrieder, S. Early detection of cancer using circulating tumor DNA: Biological, physiological and analytical considerations. *Crit. Rev. Clin. Lab. Sci.* <https://doi.org/10.1080/10408363.2019.1700902> (2019).
- Vidal, J., Taus, A. & Montagut, C. Dynamic treatment stratification using ctDNA. *Recent Results Cancer Res.* **215**, 263–273. https://doi.org/10.1007/978-3-030-26439-0_14 (2020).
- Pös, O., Biró, O., Szemes, T. & Nagy, B. Circulating cell-free nucleic acids: Characteristics and applications. *Eur. J. Human Genet.* **26**(7), 937–945. <https://doi.org/10.1038/s41431-018-0132-4> (2018).
- Oellerich, M., Schütz, E., Beck, J. & Walson, P. D. Circulating cell-free DNA-diagnostic and prognostic applications in personalized cancer therapy. *Ther. Drug Monit.* **41**(2), 115–120. <https://doi.org/10.1097/FTD.0000000000000566> (2019).
- Stewart, C. M. & Tsui, D. Circulating cell-free DNA for non-invasive cancer management. *Cancer Genet.* **228–229**, 169–179. <https://doi.org/10.1016/j.cancergen.2018.02.005> (2018).
- Giannopoulou, L., Kasimir-Bauer, S. & Lianidou, E. S. Liquid biopsy in ovarian cancer: Recent advances on circulating tumor cells and circulating tumor DNA. *Clin. Chem. Lab. Med.* **56**(2), 186–197. <https://doi.org/10.1515/cclm-2017-0019> (2018).
- Satyal, U., Srivastava, A. & Abbosh, P. H. Urine biopsy-liquid gold for molecular detection and surveillance of bladder cancer. *Front. Oncol.* **9**, 1266. <https://doi.org/10.3389/fonc.2019.01266> (2019).
- Finotti, A. *et al.* Liquid biopsy and PCR-free ultrasensitive detection systems in oncology (Review). *Int. J. Oncol.* **53**(4), 1395–1434. <https://doi.org/10.3892/ijo.2018.4516> (2018).
- Valpione, S. & Campana, L. Detection of circulating tumor DNA (ctDNA) by digital droplet polymerase chain reaction (dd-PCR) in liquid biopsies. *Methods Enzymol.* **629**, 1–15. <https://doi.org/10.1016/bs.mie.2019.08.002> (2019).
- Kwapisz, D. The first liquid biopsy test approved. Is it a new era of mutation testing for non-small cell lung cancer?. *Ann. Transl. Med.* **5**(3), 46. <https://doi.org/10.21037/atm.2017.01.32> (2017).
- Mesure, D., Drak Alsbai, K., Nicolas, A., Bieche, I. & Morillon, A. Long noncoding RNAs as new architects in cancer epigenetics, prognostic biomarkers, and potential therapeutic targets. *Biomed. Res. Int.* <https://doi.org/10.1155/2015/320214> (2015).
- Kim, H. K., Yeom, J. H. & Kay, M. A. Transfer RNA-derived small RNAs: Another layer of gene regulation and novel targets for disease therapeutics. *Mol. Ther.* <https://doi.org/10.1016/j.yjth.2020.09.013> (2020).
- Mitchell, P. *et al.* Circulating microRNAs as stable blood-based markers for cancer detection. *Proc. Natl. Acad. Sci. USA* **105**(30), 10513–10518. <https://doi.org/10.1073/pnas.0804549105> (2008).
- Aggarwal, V., Priyanka, K. & Tuli, H. S. Emergence of circulating microRNAs in breast cancer as diagnostic and therapeutic efficacy biomarkers. *Mol. Diag. Ther.* **24**(2), 153–173. <https://doi.org/10.1007/s40291-020-00447-w> (2020).
- Poller, W. *et al.* Non-coding RNAs in cardiovascular diseases: Diagnostic and therapeutic perspectives. *Eur. Heart J.* **29**, 2704–2716. <https://doi.org/10.1093/eurheartj/ehx165> (2018).
- Ambros, V. MicroRNAs: Tiny regulators with great potential. *Cell* **107**, 823–826 (2001).
- Bartel, D. P. MicroRNAs: Genomics, biogenesis, mechanism, and function. *Cell* **116**, 281–297 (2004).
- Mall, C., Rocke, D. M., Durbin-Johnson, B. & Weiss, R. H. Stability of miRNA in human urine supports its biomarker potential. *Biomark. Med.* **7**(4), 623–631. <https://doi.org/10.2217/bmm.13.44> (2013).
- Alles, J. *et al.* An estimate of the total number of true human miRNAs. *Nucleic Acids Res.* **47**(7), 3353–3364. <https://doi.org/10.1093/nar/gkz097> (2019).
- See in Wikipedia under microRNA/disease.
- Farazi, T. A., Hoell, J. I., Morozov, P. & Tuschl, T. MicroRNAs in human cancer. *Adv. Exp. Med. Biol.* **774**, 1–20. https://doi.org/10.1007/978-94-007-5590-1_1 (2013).
- Pogribny, I. P. MicroRNAs as biomarkers for clinical studies. *Exp. Biol. Med.* **243**(3), 283–290. <https://doi.org/10.1177/1535370217731291> (2017).
- Rupaimoole, R. & Slack, F. J. MicroRNA therapeutics: Towards a new era for the management of cancer and other diseases. *Nat. Rev. Drug Discov.* **16**(3), 203–222. <https://doi.org/10.1038/nrd.2016.246> (2017).
- Raabe, C., Tang, T., Brosius, J. & Rozhdestvensky, T. Biases in small RNA deep sequencing data. *Nucleic Acids Res.* **42**(3), 1414–1426. <https://doi.org/10.1093/nar/gkt1021> (2014).
- Ferracin, M. & Negrini, M. Quantification of circulating microRNAs by droplet digital PCR. *Methods Mol. Biol. (Clifton, N.J.)* **1768**, 445–457. https://doi.org/10.1007/978-1-4939-7778-9_25 (2018).

26. Valihrach, L., Androvic, P. & Kubista, M. Circulating miRNA analysis for cancer diagnostics and therapy. *Mol. Aspects Med.* **72**, 100825. <https://doi.org/10.1016/j.mam.2019.10.002> (2020).
27. Gines, G., Menezes, R., Xiao, W., Rondelez, Y. & Taly, V. Emerging isothermal amplification technologies for microRNA biosensing: Applications to liquid biopsies. *Mol. Aspects Med.* **72**, 100832. <https://doi.org/10.1016/j.mam.2019.11.002> (2020).
28. Kasianowicz, J. J., Brandin, E., Branton, D. & Deamer, D. W. Characterization of individual polynucleotide molecules using a membrane channel. *Proc. Natl. Acad. Sci. USA* **93**, 13770–13773 (1996).
29. Butler, T. Z., Gundlach, J. H. & Troll, M. Ionic current blockades from DNA and RNA molecules in the alpha-hemolysin nanopore. *Biophys. J.* **93**, 3229–3240. <https://doi.org/10.1529/biophysj.107.107003> (2007).
30. Maglia, G., Heron, A. J., Stoddart, D., Japrun, D. & Bayley, H. Analysis of single nucleic acid molecules with protein nanopores. *Methods Enzymol.* **475**, 591–623. [https://doi.org/10.1016/S0076-6879\(10\)75022-9](https://doi.org/10.1016/S0076-6879(10)75022-9) (2010).
31. Haque, F., Li, J., Wu, H. C., Liang, X. J. & Guo, P. Solid-state and biological nanopore for real-time sensing of single chemical and sequencing of DNA. *Nano Today* **8**, 56–74. <https://doi.org/10.1016/j.nantod.2012.12.008> (2013).
32. Fuller, C. W. *et al.* Real-time single-molecule electronic DNA sequencing by synthesis using polymer-tagged nucleotides on a nanopore array. *Proc. Natl. Acad. Sci. USA* **113**(19), 5233–5238. <https://doi.org/10.1073/pnas.1601782113> (2016).
33. Laszlo, A. H. *et al.* Decoding long nanopore sequencing reads of natural DNA. *Natl. Biotechnol.* **32**, 829–833. <https://doi.org/10.1038/nbt.2950> (2014).
34. Oxford Nanopore Technologies website: Nanoporetech.com, under Resources/Publications.
35. Cao, B. *et al.* Structure of the nonameric bacterial amyloid secretion channel. *Proc. Natl. Acad. Sci. USA* **111**(50), E5439–E5444. <https://doi.org/10.1073/pnas.1411942111> (2014).
36. Chen, X., Wang, L. & Lou, J. Nanotechnology strategies for the analysis of circulating tumor DNA: A review. *Med. Sci. Monit.* **26**, e921040. <https://doi.org/10.12659/MSM.921040> (2020).
37. Chaudhary, V., Jangra, S. & Yadav, N. R. Nanotechnology based approaches for detection and delivery of microRNA in healthcare and crop protection. *J. Nanobiotechnol.* **16**, 40. <https://doi.org/10.1186/s12951-018-0368-8> (2018).
38. Wanunu, M. *et al.* Rapid electronic detection of probe-specific microRNAs using thin nanopore sensors. *Nat. Nanotechnol.* **5**(11), 807–814. <https://doi.org/10.1038/nnano.2010.202> (2010).
39. Gu, L. Q. & Wang, Y. Nanopore single-molecule detection of circulating microRNAs. *Methods Mol. Biol.* **1024**, 255–268. https://doi.org/10.1007/978-1-62703-453-1_21 (2013).
40. Arata, H., Hosokawa, K. & Maeda, M. Rapid sub-attomole microRNA detection on a portable microfluidic chip. *Anal. Sci.* **30**(1), 129–135. <https://doi.org/10.2116/analsci.30.129> (2014).
41. Henley, R. Y., Vazquez-Pagan, A. G., Johnson, M., Kanavarioti, A. & Wanunu, M. Osmium-based pyrimidine contrast tags for enhanced nanopore-based DNA base discrimination. *PLoS One* **10**(12), e0142155. <https://doi.org/10.1371/journal.pone.0142155> (2015).
42. Xi, D. *et al.* Nanopore-based selective discrimination of microRNAs with single-nucleotide difference using locked nucleic acid-modified probes. *Anal. Chem.* **88**, 10540–10546. <https://doi.org/10.1021/acs.analchem.6b02620> (2016).
43. Zahid, O. K., Wang, F., Ruzicka, J. A., Taylor, E. W. & Hall, A. R. Sequence-specific recognition of microRNAs and other short nucleic acids with solid-state nanopores. *Nano Lett.* **16**(3), 2033–2039. <https://doi.org/10.1021/acs.nanolett.6b00001> (2016).
44. Ding, Y. & Kanavarioti, A. Single pyrimidine discrimination during voltage-driven translocation of osmylated oligodeoxynucleotides via the α -hemolysin nanopore. *Beilstein J. Nanotechnol.* **7**, 91–101. <https://doi.org/10.3762/bjnano.7.11> (2016).
45. Tian, K., Shi, R., Gu, A., Pennella, M. & Gu, L. Q. Polycationic probe-guided nanopore single-molecule counter for selective miRNA detection. *Methods Mol. Biol. (Clifton N.J.)* **1632**, 255–268. https://doi.org/10.1007/978-1-4939-7138-1_17 (2017).
46. Zhang, Y., Rana, A., Stratton, Y., Czyzyk-Krzeska, M. F. & Esfandiari, L. Sequence-specific detection of microRNAs related to clear cell renal cell carcinoma at fM concentration by an electroosmotically driven nanopore-based device. *Anal. Chem.* **89**(17), 9201–9208. <https://doi.org/10.1021/acs.analchem.7b01944> (2017).
47. Huang, G., Willems, K., Soskine, M., Wloka, C. & Maglia, G. Electro-osmotic capture and ionic discrimination of peptide and protein biomarkers with FraC nanopores. *Nat. Commun.* **8**(1), 935. <https://doi.org/10.1038/s41467-017-01006-4> (2017).
48. Galenkamp, N. S., Soskine, M., Hermans, J., Wloka, C. & Maglia, G. Direct electrical quantification of glucose and asparagine from bodily fluids using nanopores. *Nat. Commun.* **9**, 1. <https://doi.org/10.1038/s41467-018-06534-1> (2018).
49. Sultan, M. & Kanavarioti, A. Nanopore device-based fingerprinting of RNA oligos and microRNAs enhanced with an osmium tag. *Sci. Rep.* **9**(1), 14180. <https://doi.org/10.1038/s41598-019-50459-8> (2019).
50. Cao, C. *et al.* Single-molecule sensing of peptides and nucleic acids by engineered aerolysin nanopores. *Nat. Commun.* **10**, 4918. <https://doi.org/10.1038/s41467-019-12690-9> (2019).
51. Hao, W., Haoran, T., Cheng, Y. & Yongxin, L. Selective single molecule nanopore sensing of microRNA using PNA functionalized magnetic core-shell Fe₃O₄-Au nanoparticles. *Anal. Chem.* **91**(12), 7965–7970. <https://doi.org/10.1021/acs.analchem.9b02025> (2019).
52. Workman, R. E. *et al.* Nanopore native RNA sequencing of a human poly(A) transcriptome. *Nat Methods* **16**(12), 1297–1305. <https://doi.org/10.1038/s41592-019-0617-2> (2019).
53. Wilson, B. D., Eisenstein, M. & Soh, H. T. High-fidelity nanopore sequencing of ultra-short DNA targets. *Anal. Chem.* **91**, 6783–6789. <https://doi.org/10.1021/acs.analchem.9b00856> (2019).
54. Kanavarioti, A. Osmylated DNA, a novel concept for sequencing DNA using nanopores. *Nanotechnology* **26**, 134003. <https://doi.org/10.1088/0957-4484/26/13/134003> (2015).
55. Chang, C. H., Beer, M. & Marzilli, L. G. Osmium-labeled polynucleotides. The reaction of osmium tetroxide with deoxyribonucleic acids and synthetic polynucleotides in the presence of tertiary nitrogen donor ligands. *Biochemistry* **16**(1), 33–38 (1977).
56. Palecek E. Probing DNA structure with osmium tetroxide complexes in vitro. *Methods Enzymol.* **212**, 139–155 (1992). <https://www.ncbi.nlm.nih.gov/pubmed/1518446>.
57. Reske, T., Surkus, A.-E., Duwensee, H. & Flechsig, G.-U. Kinetics of the labeling reactions of thymine, cytosine and uracil with osmium tetroxide bipyridine. *Microchim. Acta* **166**(3–4), 197–201. <https://doi.org/10.1007/s00604-009-0195-6> (2009).
58. Kanavarioti, A. *et al.* Capillary electrophoretic separation-based approach to determine the labeling kinetics of oligodeoxynucleotides. *Electrophoresis* **33**, 3529–3543. <https://doi.org/10.1002/elps.201200214> (2012).
59. Kanavarioti, A. False positives and false negatives measure less than 0.001% in labeling ssDNA with osmium tetroxide 2,2'-bipyridine. *Beilstein J. Nanotechnol.* **7**, 1434–1446. <https://doi.org/10.3762/bjnano.7.135> (2016).
60. Debnath, T. K. & Okamoto, A. Osmium tag for post-transcriptionally modified RNA. *ChemBioChem* **19**, 1653–1656. <https://doi.org/10.1002/cbic.201800274> (2018).
61. Kanavarioti, A. HPLC methods for purity evaluation of man-made single-stranded RNAs. *Sci. Rep.* **9**(1), 1019. <https://doi.org/10.1038/s41598-018-37642-z> (2019).
62. Kanavarioti, A., & Kang, A. See RNA(OsBp) event detection Python package in a public repository: https://github.com/kangaroo96/osbp_detect and for step-by-step installation instructions see here: https://github.com/kangaroo96/osbp_detect/blob/master/instructions.md
63. Li, X.-D. *et al.* Elevated plasma miRNA-122, -140-3p, -720, -2861, and -3149 during early period of acute coronary syndrome are derived from peripheral blood mononuclear cells. *PLoS One* **12**(9), e0184256. <https://doi.org/10.1371/journal.pone.0184256> (2017).

64. Thum, T. *et al.* MicroRNA-21 contributes to myocardial disease by stimulating MAP kinase signaling in fibroblasts. *Nature* **456**(7224), 980–984. <https://doi.org/10.1038/nature07511> (2008).
65. Lai, J. Y. *et al.* MicroRNA-21 in glomerular injury. *J. Am. Soc. Nephrol.* **26**(4), 805–816. <https://doi.org/10.1681/ASN.2013121274> (2015).
66. Kao, H. *et al.* Urine miR-21–5p as a potential non-invasive biomarker for gastric cancer. *Oncotarget* **8**(34), 56389–56397. <https://doi.org/10.18632/oncotarget.16916> (2017).
67. Fulci, V. *et al.* Quantitative technologies establish a novel microRNA profile of chronic lymphocytic leukemia. *Blood* **109**(11), 4944–4951. <https://doi.org/10.1182/blood-2006-12-062398> (2007).
68. Wang, Y. *et al.* Circulating miRNA-21 as a diagnostic biomarker in elderly patients with type 2 cardiorenal syndrome. *Sci. Rep.* **10**, 4894. <https://doi.org/10.1038/s41598-020-61836-z> (2020).
69. Majlessi, M., Nelson, N. C. & Becker, M. M. Advantages of 2'-O-methyl oligoribonucleotide probes for detecting RNA targets. *Nucleic Acids Res.* **26**, 2224–2229 (1998).
70. MSDS and Information is obtained from the following link to UCLA Chemistry Department, see https://www.chemistry.ucla.edu/sites/default/files/safety/sop/SOP_Osmium_Tetroxide.pdf.

Acknowledgements

We are grateful to the SBIR/NIH program for their continued support. The work, JGB, ASWK, and AK were supported by SBIR Grant 1R43HG010841 from NIH/NHGRI.

Author contributions

A.K. conceived the project, designed the study and wrote the manuscript; she conducted the nanopore, and HPLC experiments and analyzed the data. W.J. designed and conducted the enzymatic polymerization reactions. A.S.W.K. developed the *OsBp_detect* software tool. J.G.B. helped with data analysis and manuscript preparation. All four authors reviewed the manuscript.

Competing interests

Anastassia Kanavarioti has filed a non-provisional patent application as sole inventor; she is the Founder and Director of Yenos Analytical LLC, a company delivering custom analytical solutions for native, synthetic, or transcribed nucleic acids, and engaged in the development and manufacturing of labeled/tagged nucleic acids. There is no competing interest or relationship (commercial, financial, or non-financial) between the three companies, namely Oxford Nanopore Technologies, New England BioLabs, and Yenos Analytical LLC and their employees.

Additional information

Supplementary information is available for this paper at <https://doi.org/10.1038/s41598-020-76667-1>.

Correspondence and requests for materials should be addressed to A.K.

Reprints and permissions information is available at www.nature.com/reprints.

Publisher's note Springer Nature remains neutral with regard to jurisdictional claims in published maps and institutional affiliations.



Open Access This article is licensed under a Creative Commons Attribution 4.0 International License, which permits use, sharing, adaptation, distribution and reproduction in any medium or format, as long as you give appropriate credit to the original author(s) and the source, provide a link to the Creative Commons licence, and indicate if changes were made. The images or other third party material in this article are included in the article's Creative Commons licence, unless indicated otherwise in a credit line to the material. If material is not included in the article's Creative Commons licence and your intended use is not permitted by statutory regulation or exceeds the permitted use, you will need to obtain permission directly from the copyright holder. To view a copy of this licence, visit <http://creativecommons.org/licenses/by/4.0/>.

© The Author(s) 2020